1-1-2009

Visualization of an internal sand displacement field around a laterally loaded vertical pile

Ranga Walakulu Arachchi
Ryerson University

VISUALIZATION OF AN INTERNAL SAND DISPLACEMENT FIELD AROUND A LATERALLY LOADED VERTICAL PILE

by

Ranga Walakulu Arachchi
BSc. Eng (Hons)
University of Peradeniya, 1999

A thesis
presented to Ryerson University

in partial fulfillment of the
requirements for the degree of
Masters of Applied Science
in the Program of
Civil Engineering

Toronto, Ontario, Canada, 2009

AUTHOR'S DECLARATION

I hereby declare that I am the sole author of this thesis.

I authorize Ryerson University to lend this thesis to other institutions or individuals for the purpose of scholarly research.

I further authorize Ryerson University to reproduce this thesis by photocopying or by other means, in total or in part, at the request of other institutions or individuals for the purpose of scholarly research.

To my dear wife Nalana,

two sons Malisha and Nisal

for their support, encouragement and Love

ACKNOWLEDGEMENT

This research could not have been accomplished without the assistance of a number of individuals. I would like to thank my supervisor Dr. Jinyuan Liu for his guidance, advice, and the encouraging comments. In two years of work Dr. Liu always had insightful opinions that reshaped my thinking and analysis processes. His contribution and the constructive comments in the preparation of this thesis is greatly appreciated.

I am very thankful to Dr. Arnold Yuan and Dr. Ahamed Shaker their valuable and constructive comments to improve some of the chapters in the thesis.

I am very grateful to the civil engineering department at Ryerson University for supporting me and funding for the research work.

I am very thankful to Ms. Hongmei Gao for her support in thesis formatting and encouragement during the difficult times. I greatly appreciate Mr. Minglaing Liu for his huge contribution in the development of the lateral loading arrangement with the data acquisition system and software support.

I am very thankful to Mr. Chratien Mak for programming the CCD camera using Matlab for self image capturing and to Mr. Sunil Perera for making some test components.

The administration support and the friendly advice from Ms. Kim Kritzer is dearly remembered. I am also very thankful to Mr. Myuran Balasubramanium (PEng) and Mr. Tharani Thangavadivel (PEng) for their motivation, advice and material support .

I must remember Prof. Wanghua Sui for his valuable advice and capturing some important moments during the test.

Finally I dearly remember my wife, and the two sons for their commitment and encouragement during this exercise.

ABSTRACT

VISUALIZATION OF AN INTERNAL SAND DISPLACEMENT FIELD AROUND A LATERALLY LOADED VERTICAL PILE

By

Ranga Walakulu Arachchi
Masters of Applied Science, Civil Engineering

In this research, an internal sand displacement field around a laterally loaded vertical pile is visualized using transparent soil and an image processing technique called digital image cross-correlation (DIC). DIC is a region-based image processing technique which can calculate the displacement field between two images. Transparent soil is made of silica gel with a pore fluid having the same refractive index. Transparent soil has been studied to have the strength and deformation properties similar to natural soil. An optical test set-up is developed to capture the images during loading. This optical test set-up consists of a camera, a laser light, a line generator lens, a loading frame, a Plexiglas mould, and a PC. The saturated fine sand in loose condition is modeled in this research. A laser light sheet is generated to slice the transparent soil model by passing a laser beam through the line generator lens. A distinctive laser speckle pattern is generated through the interaction between the laser light and transparent soil. A series of images are taken from the camera while a scaled pile is being loaded laterally. The displacement fields are calculated by cross-correlating two consecutive images and the corresponding strain fields are deduced from the displacement fields. The development of both displacement and strain fields is investigated by studying deformation and strains at different loading stages. The test results are similar to the published data. This research improves the understanding of soil movement around a laterally loaded pile. It also advances the physical modeling technique using transparent soil.

TABLE OF CONTENTS

LIST OF TABLES

LIST OF FIGURES

CHAPTER 1

INTRODUCTION

1.1 LATERALLY LOADED PILE

Almost all the piled foundations are subjected to at least some degree of horizontal loading. In many cases, the magnitude of the loads in relation to the applied vertical loading is so small that, no additional design calculations are necessary for the lateral effect. For example, the piled foundation of a building with a moderate height will easily withstand the small wind loading that the building will be subjected to. Traditionally, piles are installed at an angle to the vertical and in such cases lateral resistance is efficiently provided by the horizontal component of the axial loading capacity. Therefore in most cases it is very conservative to ignore the lateral loading effect.

But in some cases, such as offshore platforms, wind farms, transmission lines, microwave towers, highways and variety of units in industrial plants, horizontal loading may prove to be very critical in the design (Tomlinson and Woodward, 2008). The currents, waves, winds, floating ice, berthing ships etc. are sources of very dominant horizontal loading.

The performance and behavior of laterally loaded piles have been under investigation for many decades. Gleser (1953), Reese and Matlock (1956), Matlock and Reese (1960) have presented different approaches to the solution of lateral behavior of vertical piles under horizontal loading.

In practice, many structures are supported by groups of piles, the analyses of pile groups under lateral loading start with the analysis of single pile; soil responses are then modified according to the pile spacing (Reese et al. 2006). In order to simplify the problem, this research focuses on the soil-structure interaction related to a single pile.

The response of soil around a laterally loaded pile is influenced by the loading type: static and dynamic. Only the static loading case will be studied in this research. In order to accurately predict the behavior of a laterally loaded pile for a more efficient and economical design of the piles, it is very important to know the behavior of soil around the pile and its variation with loading. But so far no attempts have been made to visualize the actual behavior of inside soil around the pile when loaded laterally.

1.2 SCOPE OF STUDY

In this research, an internal soil displacement field around a laterally loaded pile is visualized using transparent soil and an image processing technique called digital image cross-correlation (DIC). DIC is a region-based image processing technique which can calculate the displacement field between two images. Transparent soil is made of silica gel with a pore fluid having the same refractive index. Transparent soil has been studied to have the strength and deformation properties similar to natural soil.

An optical test set-up is developed in order to capture the images during loading. This optical set-up consists of a complimentary metal-oxide semiconductor (CMOS) camera, a laser light, a line generator lens, a loading frame, a Plexiglas box, and a PC. A saturated fine sand sample in loose conditions is modeled in this research. A laser light sheet is generated to slice the transparent soil model by passing a laser beam through the line generator lens. A distinctive laser speckle pattern is generated through the interaction between the laser light and transparent soil. A series of images are taken with the camera while a scaled pile is being loaded laterally using the horizontal loading arrangement which consists of a loading cell and a LVDT. The displacement fields are analyzed using a PIV software. The development of both displacement and strain fields are investigated by studying images at different loading stages.

1.3 OBJECTIVES

- Model transparent soil with silica gel to simulate the condition in loose sand
- Investigate geotechnical properties of transparent soil
- Study the displacement and strain field around a laterally loaded pile

1.4 TRANSPARENT SOIL

The main objective of this experiment is to visualize an internal displacement field around a laterally loaded pile installed in sand, using transparent soil. Mannheimer and Oswald (1993) and Iskander et al. (1994) demonstrated that the transparent substances made of amorphous silica powder and a pore fluid with a matching refractive index exhibit macroscopic geotechnical properties similar to natural clay. Later another type of transparent soil made of silica gel was developed to model sand (Sadek et al., 2002). Both kinds have the same refractive index, which permits transparent soil to model the layered conditions in the field. Transparent soil has been studied to have strength and deformation properties similar to natural soil (Sadek et al. 2002).

In this research, the second type of transparent soil is used to simulate sand. Silica gel is a colloidal form of silica. It is inert and porous and is available in wide range of grain size. The size of silica used for this experiment is in the range of 0.5 mm to 1.5 mm and referred to as fine silica. The typical stress – strain behavior for fine silica gels is consistent with that of sand (Iskander et al. 2002b, Sadek 2002).

1.5 OPTICAL SETUP

An optical test set-up is developed to capture the deformation during loading, which consists of a CMOS camera, a laser light, a line generator lens, a loading frame, a Plexiglas box and a PC. A laser light sheet is generated to slice the transparent soil model by passing a laser beam through the generator lens. A distinctive laser speckle pattern is generated through the interaction between the laser light and transparent soil. A series of images are taken from the camera while a scaled pile is being loaded laterally.

1.6 DIGITAL IMAGE PROCESSING

In this research, a region based image processing technique called digital image cross correlation (DIC) is used to calculate the displacement field between two images.

This is a non- intrusive optical technique and has been widely used in many engineering fields to obtain spatial deformation patterns, albeit with several names. It

is also known as particle image velocimetry in fluid dynamics measurement (Adrian 1991), surface displacement analysis in solid mechanics (Sutton et al 1983). DIC has recently been used for monitoring soil deformations during shear. Image subtracting was used by Allersma (1997) to measure deformation of a slope in field.

1.7 STRUCTURE OF THESIS

This thesis is about a visualization technique of an internal displacement field around a laterally loaded pile in sand. The Thesis consists of seven chapters. Chapter 1 basically explains the scope, objectives and an introduction of the research. Chapter 2 consists of the behavioral aspects of soil around a laterally loaded vertical pile. Chapter 3 discusses about the synthetic soil, its properties and suitability to represent sand. Chapter 4 briefly explains the theory behind the DIC which is the imaging technique used in the PIV software to calculate displacements using the images. Chapter 5 discusses about the experimental setup and the test procedure. Chapter 6 is about data analyzing using PIV software and results. Chapter 7 provides conclusions and recommendation for future research.

CHAPTER 2

SOIL RESISTANCE AROUND A LATERALY LOADED VERTICAL PILE

2.1 INTRODUCTION

Horizontal loads on a vertical pile are resisted by the mobilization of resistance in the surrounding soils, as the pile deflects. The lateral load capacity of the pile depends essentially on the combination of the stiffness of the pile and of the resistance of the surrounding soil to the imposed loads.

The horizontal load capacity of vertical piles may be limited in three different ways: the capacity of the soil may be exceeded, resulting the large horizontal movements of the piles and the failure of the foundation, the bending moments may generate excessive bending stresses in the pile material, resulting in structural failure of the piles; or the deflections of the pile heads may be too large to be compatible with the superstructure. All three methods of failure must be considered in design.

The methods presently available for the design of piled foundations subjected to horizontal loads must be regarded as highly empirical. The input soil data are associated with a high degree of uncertainty. Therefore, these methods must be used with great caution and with due consideration of their limitation.

There is a lateral pressure from surrounding soil which is applied on the file skin area. During lateral loading, the soil pressure changes with pile deformation.

The analysis of this problem is complex due to the high non-linearity of the soil stress-strain behavior. The lateral pile response is also non-linear, even for low levels of applied load.

This has been shown in previous experimental studies (Matlock, 1970; Murchison and O'Neill, 1984; Kim, 1997) and has led to the use of non-linear methods of analysis.

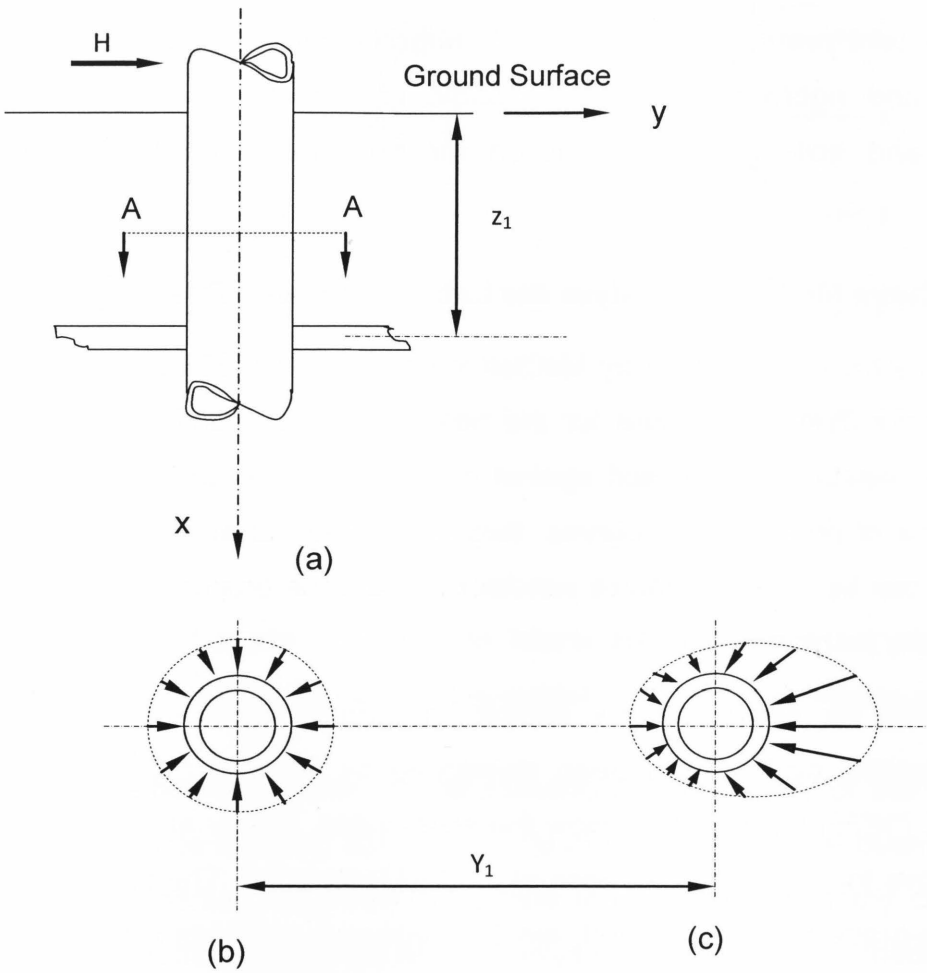

Figure 2.1 Distribution of unit stress against a pile before and after lateral deflection: (a) elevation view of section of pile. (b) Earth pressure prior to lateral loading. (c) Earth pressure after lateral loading

Several methods of analyzing laterally loaded piles are available and some of them are, sub-grade reaction method, elastic continuum method and *p-y curve* method. Out of these the p-y curve method is the most commonly used analytical tool by practicing engineers.

Extensive research has been devoted to the derivation and recommendation of *p-y* curves for different soils e.g., Dunnavant and O'Neill 1989; Reese and Van Impe 2000. Apart from being a simple and reasonably accurate solution, the *p-y* method's ability to model soil nonlinearity makes it superior to the sub-grade reaction method. In recent years, the finite element method (FEM) has gained recognition as a versatile and rigorous technique, capable of modeling soil nonlinearity, soil continuum, and soil-structure interaction for both two- and three dimensional problems.

2.2 P-Y Curve Method to Analyze the Laterally Loaded Piles

The *p-y* method, devised by McClelland and Focht (1958), appears to be the most practically useful procedure for the design of deep foundations under lateral loading. The resistance of the soil against the pile is related to the deflection of the pile by means of nonlinear *p-y* curves. Because numerical analyses are employed, this method can be used to analyze conditions where the properties of the soil or the pile vary in any fashion with depth.

Methods for estimating *p-y* curves for various types of soil and loading conditions (static, cyclic) have been developed by Matlock (1970) for soft clay, Reese et al. (1975) for stiff clay below the water table, Reese and Welch (1975) for stiff clay above the water table, Reese et al. (1974) for sand. The analytical methods such as sub-grade reaction method, elastic continuum methods are applicable only to the deflections of piles which are within the range of the elastic compression of the soil caused by the lateral loading on the piles. These analytical methods however, can be extended beyond the elastic range to analyze movements where the soil yields plastically up to and beyond the stage of shear failure.

This can be done with the extension of the sub-grade reaction method to include non-linear springs for representing the non-linear behavior of soil. In place of a coefficient of sub-grade reaction, a complete load transfer (p- load per unit length of pile, *y*- deflection) curve can be specified and with the use of modern computer techniques solution can be found easily.

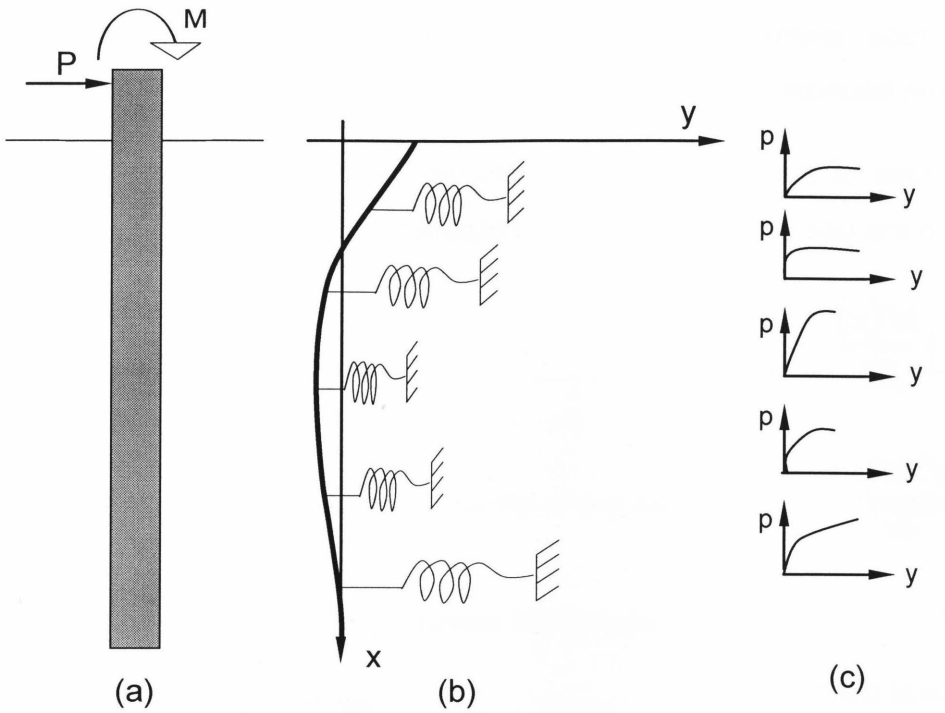

Figure 2.2 Model of a pile subjected to lateral loading with a set of p-y curves: (a) pile under lateral loading.(b) soil spring model.(c) p-y curves (Reese et al. 2006)

As *p-y* method is capable of representing a wide variety of soil and loading conditions in a simple manner, and the results of *p-y* method have been found to be in reasonable agreement with results of field loading tests in many cases, these analyses represent the state-of-the art for analysis of single laterally loaded piles and drilled shafts. But the important problem of the *p-y* method is the selection of reasonable values of the modulus of soil resistance (E_s) and ultimate soil resistance (P_u) in a given case.

In order to check the effectiveness of p-y curve method for predicting the behavior of laterally loaded piles in sand (Reese et al., 1974) for sand, full sized field tests were done and both static and cyclic loading were employed.

For each type of loading, a series of lateral loads were applied beginning with a small magnitude, and a set of bending moment curves were obtained associated with the suitable boundary conditions.

The values of p and y along the pile can be obtained solving the following equations, with the use of plotted bending moment curves.

$$y = \iint \frac{M(x)}{EI} \qquad \text{Eq (2-1)}$$

$$p = \frac{d^2 M(x)}{dx^2} \qquad \text{Eq (2-2)}$$

Where

y - Lateral deflection

p - Soil resistance

M(x) - Bending moment

E – Modulus of elasticity of pile material

I - Second moment of area of the pile

Equations must be solved numerically with the appropriate boundary conditions. The solution of Equation (2-1) can be normally obtained to the required accuracy, but an analytical difficulty is encountered in the solution of Equation (2-2). In this study, it has been assumed that the soil modulus could be described as a function of depth by a two-parameter non-linear curve. The two parameters were computed from the experimental data, allowing the soil reaction curve to be computed analytically.

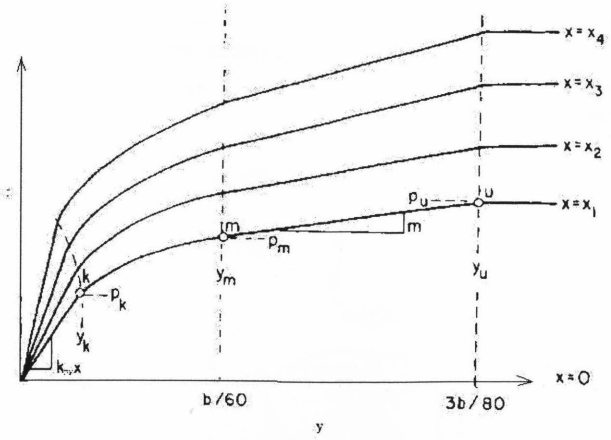

Figure 2.3 Characteristic shape of a family of p-y curves for static loading in sand

2.3 Recommendation of p-y curves for Sands

2.3.1 Initial portion of curves

The initial stiffness of stress-strain curves for sand is a function of the confining pressure; therefore, the use of mechanics for obtaining E_{pymax} for sands is complicated. The p-y curve at the ground surface will be characterized by zero values of p for all values of y, and the initial slope of the curves and the ultimate resistance will increase approximately linearly with depth.

The recommendations for the initial portion of the p-y curves for sand were derived from field tests . Terzaghi (1955) presented values that were useful in form, that is, starting with zero at the groundline and increasing linearly with depth. However, his values were for the case where the computed value of p would be equal to one-half of the ultimate bearing stress. Field tests suggested the recommendations in the following table.

Table 2.1 Suggested Values of K_p for Sands (Terzaghi, 1955)

Relative Density of Sand	Loose	Medium	Dense
	Submerged Sand		
MN/ m^3	5.4	16.3	34.0
Psi/in	20.0	60.0	125.0
	Sand above water table		
MN/ m^3	6.8	24.4	61.0
Psi/in	25.0	90.0	225.0

2.3.2 Ultimate resistance (p_u) for sands

Two models can be used to gain some insight into the ultimate resistance $\mathbf{P_u}$ that may develop as a pile is deflected laterally.

The first model assumes that the sand will move up and out at the ground surface; the second model takes over below the first and assumes horizontal movement of the sand.

The first model for the soil resistance near the ground surface is shown in Figure 2.4. The total lateral force F_{pt} (Figure 2.4c) may be computed by subtracting the active force F_a, computed by using Rankine theory, from the passive force F_p, computed from the model by assuming that the Mohr-Coulomb failure condition is satisfied on planes, ADE, BCF and AEFB (Figure 2.4a).

The directions of the forces are shown in Figure 2.4 b. Solutions other than the ones shown here have been developed by assuming a friction force on the surface DEFC (assumed to be zero in the analysis shown here).

Taking the weight of the wedge into account, considering the forces on the sliding surfaces the force F_{pt} may be computed expressed by following equation.

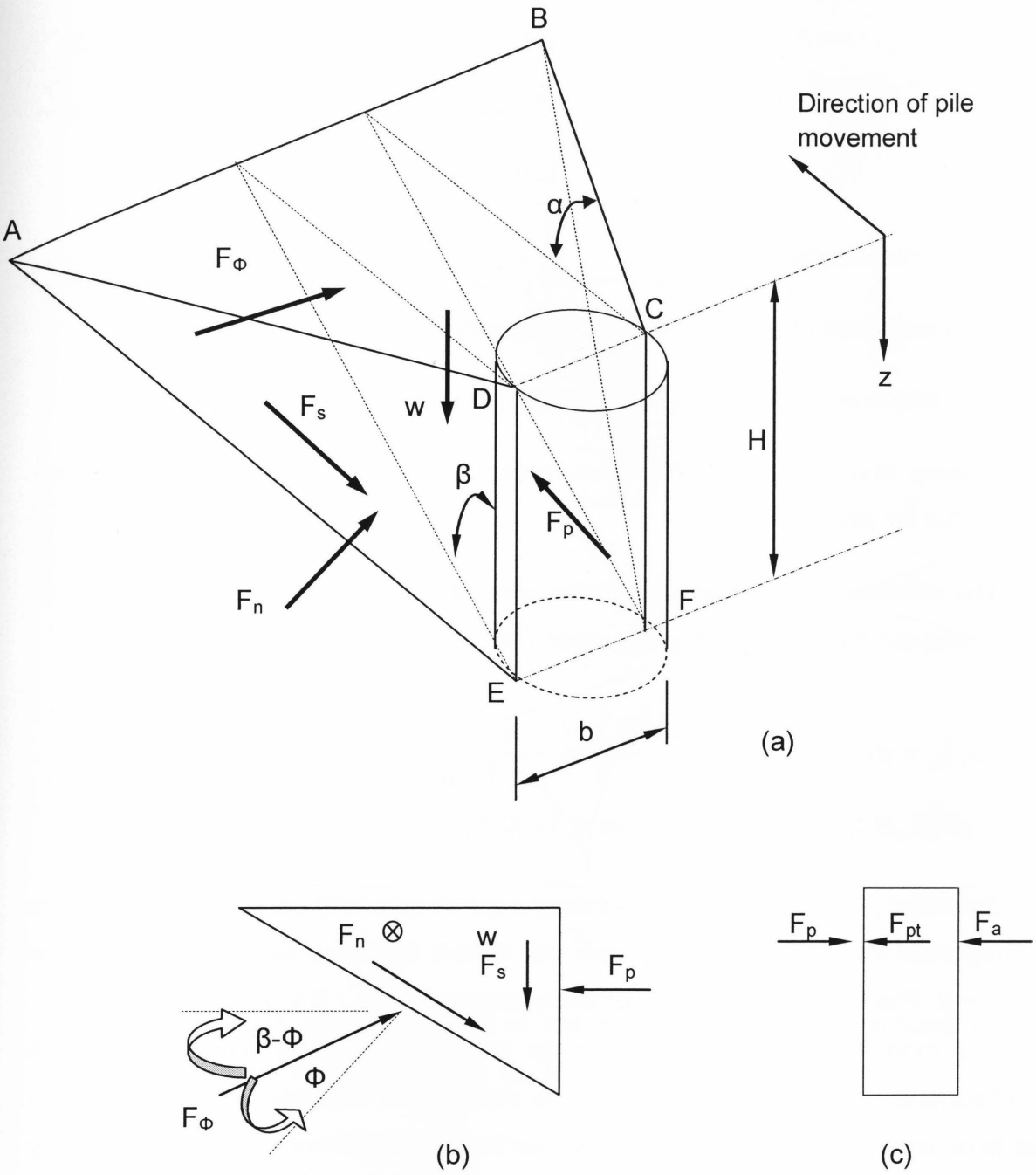

Figure 2.4 Assumed passive wedge-type failure of a pile in sand: (a) general shape of the wedge; (b) forces on the wedge ;(c) forces on the pile

$$F_{pt} = \gamma H^2 \left[\left(\frac{K_0 H \tan\phi \tan\beta}{3 \tan(\beta-\phi)\cos\alpha_s} \right) + \left(\frac{\tan\beta}{\tan(\beta-\phi)} \left(\frac{b}{2} + \frac{H}{3} \tan\beta \tan\alpha_s \right) \right) \right] + \gamma H^2 \left[\frac{K_0 H \tan\beta}{3} (\tan\phi \sin\beta - \tan\alpha_s) - \frac{K_a b}{2} \right] \quad \text{Eq (2-5)}$$

where

Φ = friction angle,

K_0= coefficient of earth pressure at rest, and

K_a = minimum coefficient of active earth pressure = $\tan^2(45 - \Phi/2)$

Sowers and Sowers (1970) have recommended K_0 values of 0.6 for loose sand and 0.4 for dense sand.

The ultimate soil resistance near the ground surface per unit length of the pile $(p_u)_{sa}$ is obtained by differentiating Equation (2-5).

$$(p_u)_{sa} = \gamma H \left[\left(\frac{K_0 H \tan\phi \tan\beta}{\tan(\beta-\phi)\cos\alpha_s} \right) + \left(\frac{\tan\beta}{\tan(\beta-\phi)} (b + H \tan\beta \tan\alpha_s) \right) \right] + \gamma H \left[K_0 H \tan\beta (\tan\phi \sin\beta - \tan\alpha_s) - K_a b \right] \quad \text{Eq (2-6)}$$

Bowman (1958) performed laboratory experiments with careful measurements and suggested values of α ranging from Φ/3 to Φ/2 for loose sand and up to Φ for dense sand. The value of β is approximately expressed by, $\beta = 45 + \Phi/2$

The model for computing the ultimate resistance at some distance below the ground surface is shown in Figure 2.5a. The stress σ_1 at the back of the pile must be equal to or larger than the minimum active earth pressure; if not, the soil could fail by slumping.

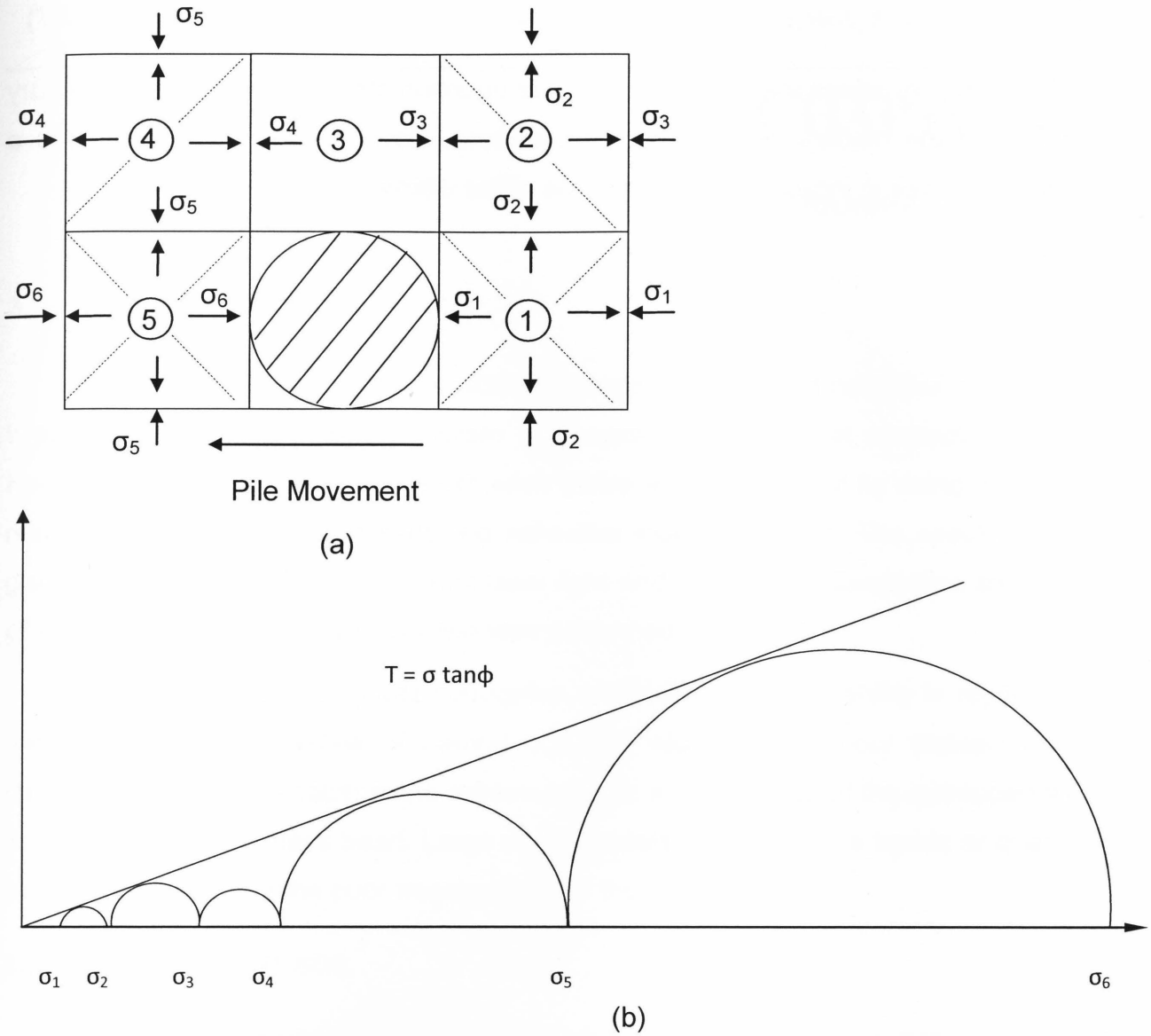

Figure 2.5 Assumed mode of soil failure by lateral flow around a pile in sand: (a) section through the pile; (b) Mohr-Coulomb diagram

The assumption is based on two-dimensional rather than three-dimensional behavior; therefore, some approximation is introduced. If the state of stress shown in Figure 2.5b is assumed, the ultimate soil resistance of sand at depth below ground surface for horizontal movement $(p_u)_{sb}$ of the soil can be expressed as,

$$(p_u)_{sb} = K_a b\gamma H\left(\tan^8 \beta - 1\right) + K_0 b\gamma H \tan\phi \tan^4 \beta \qquad \text{Eq (2-7)}$$

The equations for $(p_u)_{sa}$ and $(p_u)_{sb}$ are approximate because of the elementary nature of the models used in the computations. However, the equations serve a useful purpose in indicating the magnitude of the ultimate soil resistance.

CHAPTER 3

TRANSPARENT SOIL

3.1 INTRODUCTION

Mixing transparent materials with fluids having a matching refractive index has been attempted in the past to obtain a transparent media that resembles soils. Konagai et al. (1992) obtained deformation inside an embankment by using a model made of crushed glass and matching refractive index pore fluid. The speckle was generated by the interaction between laser light and glass bead. Qualitative analysis of images of illuminated cross-section was performed in the test.

However glass and quartz surrogates are limited by their inability to represent the geotechnical properties of natural soil and also by their poor transparency caused due to the mismatch in the refractive index and presence of the entrapped air in tiny cracks in the glass bead. Large scale models made of glass beads or quartz powder are limited by the poor transparency of the model.

3.2 TRANSPARENT SOIL

Mannheimer and Oswald (1993) and Iskander et al. (1994) demonstrated that transparent substances made of amorphous silica powder and a pore fluid with a matching refractive index exhibit macroscopic geotechnical properties similar to natural clay. Later a different kind of transparent soils made of silica gel was developed to model sand. Both materials have the same refractive index, which permits transparent soil for modeling the stratum conditions in the field.

In this research, silica gel is used to model the effect of sand. In principle, a large number of materials can be matched with suitable liquids to obtain transparent mixtures. In fact, liquids with refractive indices guaranteed to the third decimal digit can be obtained commercially. However, cost is an important consideration in choosing materials to make transparent synthetic soils.

The materials used in this research were selected, in part, because of their low cost and availability. The transparency of these aggregates is superior to crushed glass, which has been used previously. The glass does not adsorb pore fluid, and its rough sharp edges refract light.

3.2.1 What is Silica Gel?

Silica gel is a colloidal form of silica. It is inert and porous, and is available in sizes ranging from 0.5 mm to 5 mm (Figure 3.1). The most common shapes are rounded beads and angular particles. The type of silica used for the experiment is angular particles, 0.5 – 1.5 mm in size and referred to as fine silica (supplied by *Multisorb Technologies*). The typical stress-strain behavior of fine silica gels has been proven to be consistent with that of sands.

The angle of friction from triaxial test is in the range of 30°–36° for fine silica gel. Young's modulus ranges between 24 to 84 MPa depending on density and size. These values are similar to the values reported for natural sands. More details can be found in Iskander et al. (2002b), Sadek (2002), and Sadek et al.(2002).

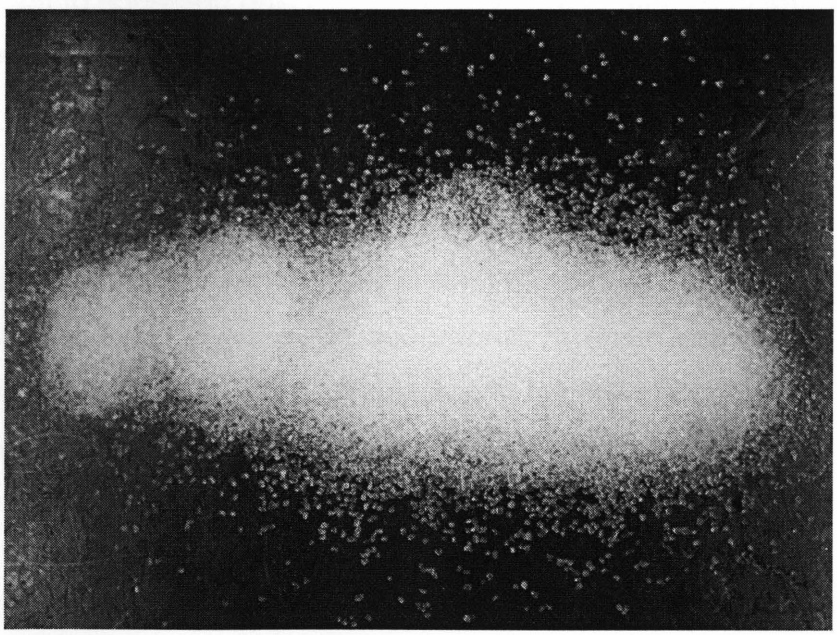

Figure3.1 Photograph of dry silica gel

3.2.2 Pore Fluids

The pore fluid was a 50:50 blend by volume of colorless mineral oil (Drakeo, K7041) and a normal-paraffinic solvent (Magiesol 47, K7544) supplied by Penreco.

These two fluids are not miscible, which permits studying multiphase flow problems such as the contamination of aquifer with petroleum products. This pore fluid has a refractive index of 1.447 at 25°C. The viscosity and density of the oil blend at a room temperature (23°C) were 5.0 cP and 804 kg/m^3, respectively.

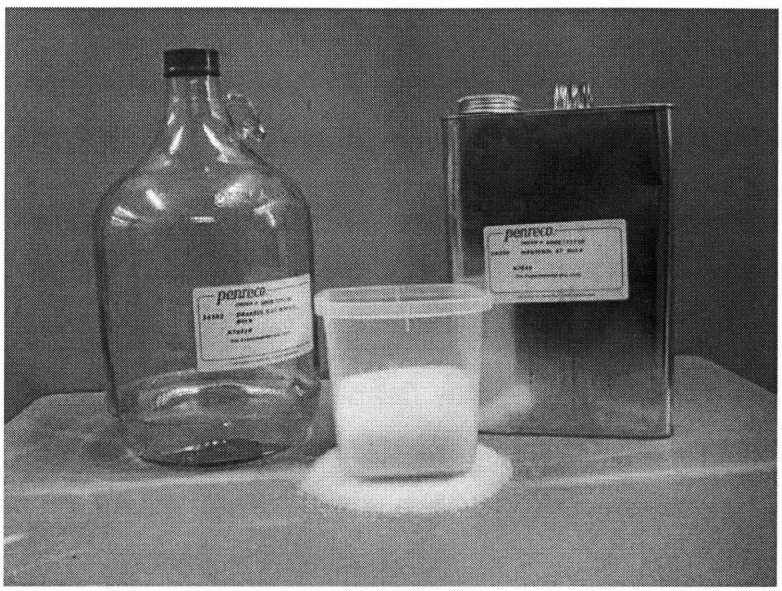

Figure 3.2 Photograph of the components used to prepare transparent soil.

3.3 PHYSICAL PROPERTIES OF SILICA GEL

The internal structure of silica gel particles is different from sands. It contains an enormous number of micro-pores. This fact affects all the physical properties that are discussed in the following sections.

3.3.1 Particle Structure

Silica gel particles are typically made from the "xerogel" mass formed during chemical reaction. This mass consists of a three dimensional vast networks made up of chains of particles that range in size from 3 – 30 nanometer, (Iler 1955).

This vast network has inter – connected pores with an average diameter of approximately 21 A^0, and totaling 0.43 cm^3 per gram of silica (Sphinx, 1993).

3.3.2 Specific Gravity and Unit Weight

The specific gravity of silica gels is 2.2 (Weast,1986), which is approximately 80% of the specific gravity natural silicate sands. The dry unit weight is 6 – 9 KN/ m^3, which depends on packing, shape and grain size. The saturated unit weight depends on the pore fluid used, and is 11- 14 KN/ m^3, for the mineral oil and solvent pore fluid used in this research.

3.3.3 Void Ratio

Void ratio calculations for silica gel are different from normal soils, because silica gel aggregates have pores inside. These in-aggregate pores should not be considered when calculating the void ratio for geotechnical engineering purposes. In this respect, silica gel is similar to silica powder.

3.3.4 Particle Size Distribution and Uniformity

The type of silica gel used was angular in the size range 0f 0.5 mm- 1.5 mm. A mechanical test (Sieve analysis) was done to verify the particle size range. Figure 3.3 shows the test results. Commercial silica gels are usually sold in uniform size ranges, i.e. the purchased silica will have a pre-defined maximum particle size. The particle size distribution graph in Figure 3.3 shows this clearly.

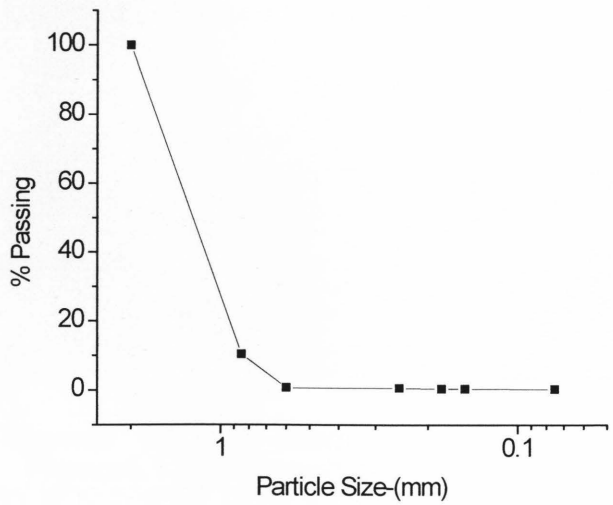

Figure 3.3 Particle distribution

The sieve analysis of tested samples shows that some particles break during shearing. Particle breakage is considered one of the main disadvantages of using silica gels for modeling natural soils.

3.4 GEOTECHNICAL PROPERTIES OF SILICA GEL

3.4.1 Shear Strength

Silica gel has been tested for its geotechnical properties in the past (Iskander et al. 2002). The friction angle (Φ) found to be in the range of 30°- 36° from a triaxial test. A direct shear test was performed to verify this result using a dry sample of silica gel and the obtained the Φ value was very close to 34°. The stress-strain behavior of silica gels is consistent with typical stress strain behavior of sand for both dense and loose conditions. Peak strength, however, is reached at higher strains than normally expected for dense sands due to the compressibility of the silica gel particles (Sadek et al. 2002 and Iskander et al. 2002).

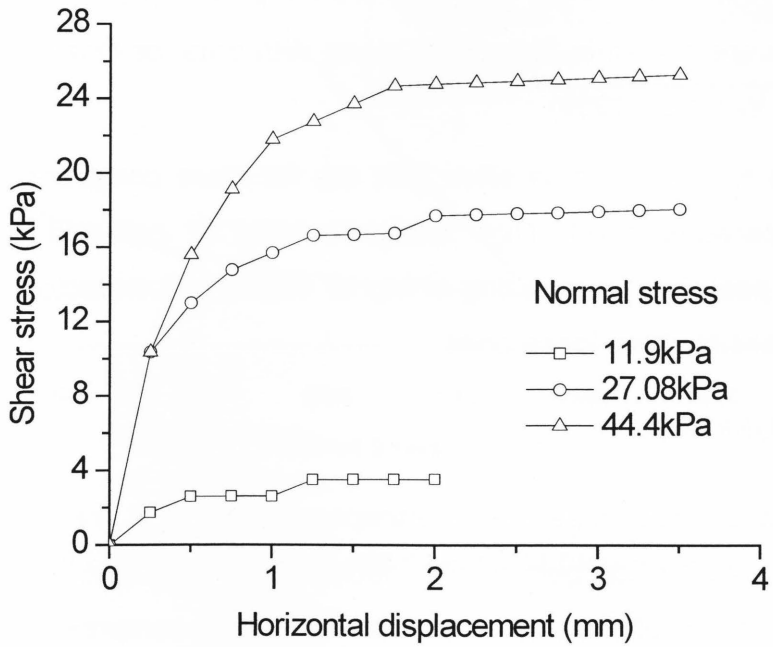

Figure 3.4 Variation of shear stress with the horizontal movement

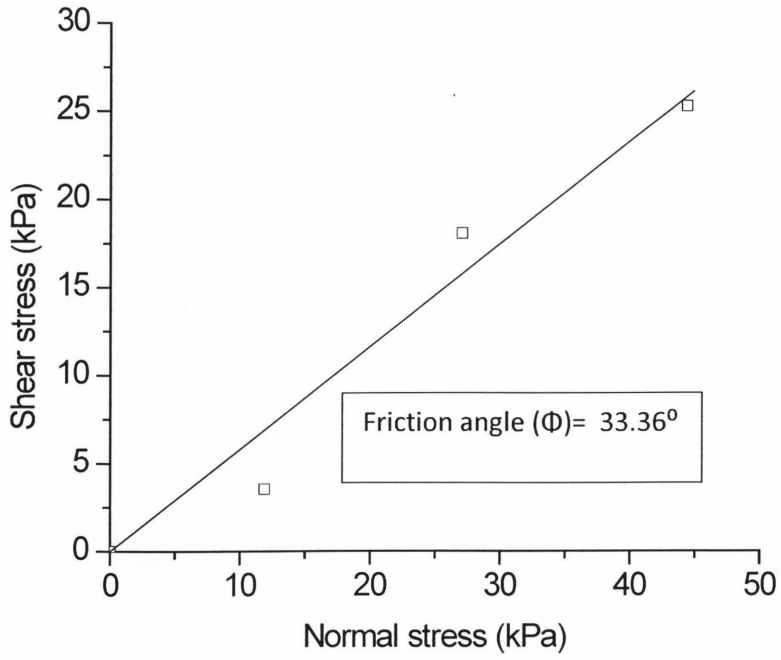

Figure 3.5 Variation of shear stress with the normal stress

3.4.2 Compressibility

A compressibility test was performed by Sadek (2002) on the same kind of silica gel (both loose and dense) using the one-dimensional consolidation apparatus. The test results are shown in Figure 3.6 along with data for Ottawa and Calcareous sands (Lamb & Whitman 1969).

Both the fine and coarse silica gels are far more compressible than Ottawa sand and calcareous sand. High compressibility is believed to contribute to phenomena of peak stress occurring at higher strains. As expected, dense samples are less compressible than loose ones.

3.5 CONCLUSIONS

The geotechnical properties of transparent silica gel are summarized in this chapter. Transparent silica gels exhibit geotechnical properties similar to those of natural sands in terms of shear strength. However, their compressibility is larger than that of typical sands. Silica gels can be used to model sands, though special caution is required in interpolating model results because of its high compressibility.

More researches are required for preventing a potential misleading interpretation of the model results from transparent soils. Researches can be explored in many aspects, including the critical stress parameters of this material, non-dimensional analysis, and surface charge influence on the geotechnical behavior of this material.

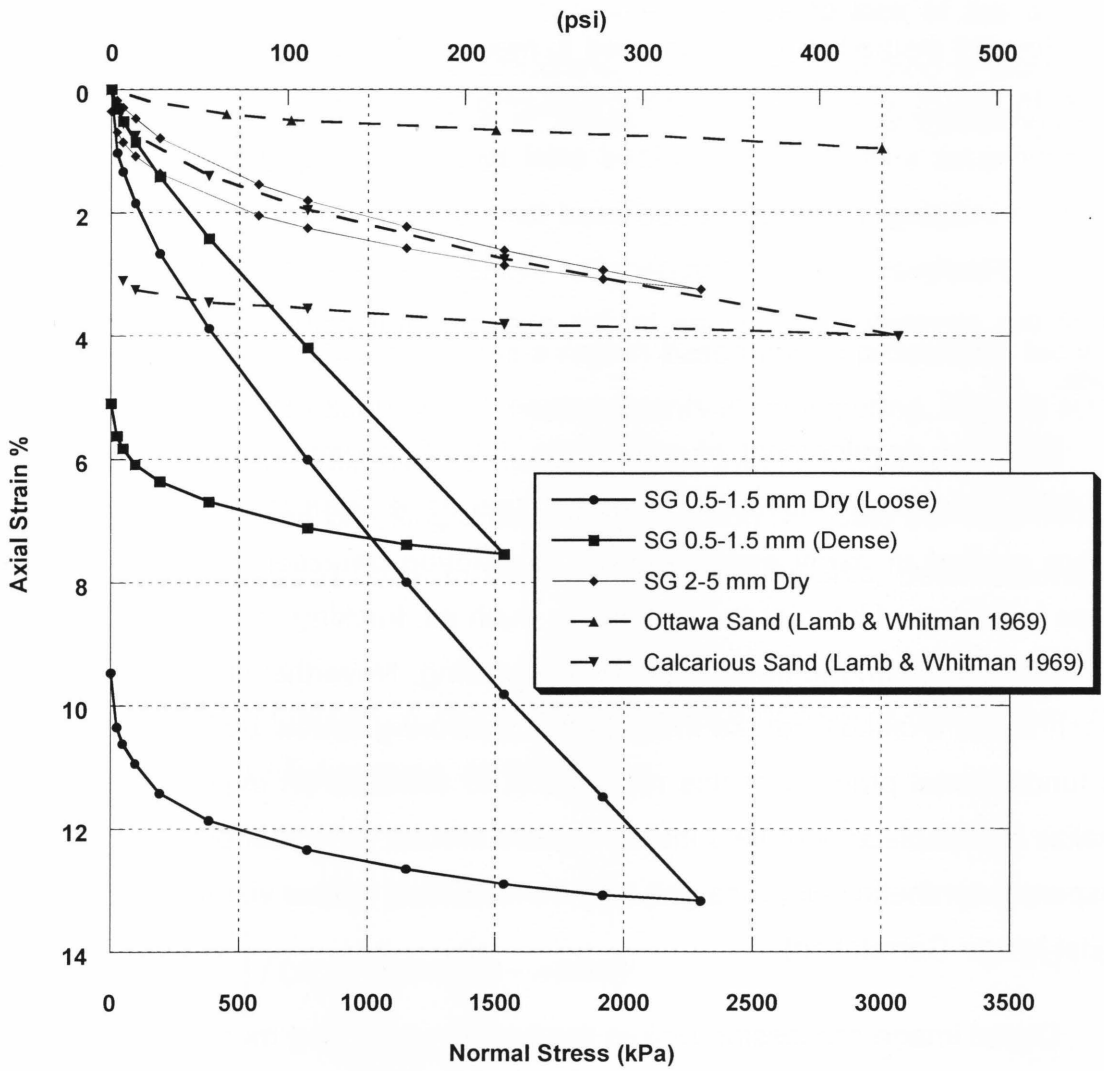

Figure 3.6 Compressibility of silica gels and natural sands (Sadek 2002)

CHAPTER 4

DIGITAL IMAGING IN GEOTECHNICAL ENGINEERING

4.1 INTRODUCTION

Several methods have been used to measure continuous spatial deformations in soils. In 1960s, x-ray was used for measuring spatial deformations. More recently, new techniques such as computerized axial tomography (CAT scan) and magnetic resonance imaging (MRI) have been used for experimental modeling of geotechnical problems. However, the broad application of these techniques is limited by the high cost of the apparatus, difficulties in the experimental setup, and interpretation of results.

With the development of computers, CMOS cameras, frame-grabbers, and laser light technology, digital image techniques have been improved tremendously and are applied in many engineering fields. Motion detection from a sequence of images has been of interest to many fields, such as, tracking of targets in the military field, traffic monitoring in transportation engineering. Nevertheless, to date there are no techniques available to use imaging for measuring spatial deformations in soils. The fundamental premise of this research is to simulate an experimental setup to visualize the displacement field inside the soil around a vertical pile with the help of transparent synthetic soil (silica gel) and non-intrusive optical visualization technique (Digital Image Correlation).

Digital image processing makes the image processing much easier and faster than the time-consuming traditional film processing. The advantages of the digital image techniques are not only that the system is easier and faster to use, but also the sequence of images are downloaded and stored in a computer individually. The stored individual images allow correlating multiple separate images rather than only an image used in traditional photography. In addition to that, each image can be pre-processed before the analysis to produce better results.

4.2 MOTION ESTIMATION METHODS

Motion estimation from a sequence of images, also referred as optical flow estimation, is performed by treating the 2-D image as a continuous mathematical function. There are basically three methods for motion estimation ;(1) Fourier method, (2) Differential Method, (3) Matching method.

An accurate numerical differentiation (differential method) may be impractical due to image noise, the small number of frames, or due to lack of the alignment between the images. Under these conditions, the matching method is more robust than the differential method (Barron et al. 1994). The most popular matching method is digital image cross-correlation (DIC).

4.3 DIGITAL IMAGE CORRELATION

Digital image correlation (DIC) is a region based image processing technique which is widely used for experimental measurements in engineering. E.g. (1) surface displacement analysis - solid mechanics, (2) particle image velocimetry (PIV) - fluid mechanics. DIC is based on using a correlation function to locate the best matching position of two images, in order to calculate body movements, deformations, and velocity profiles.

The cross-correlation function, c, of the light intensity functions of two images, *f(x,y)* and *g(x,y) = f(x+Δx, y+Δy),is given* as the follows:

$$c(\xi,\eta) = \int_{-\infty-\infty}^{+\infty+\infty} f(x,y)g(x+\xi,y+\eta)dxdy \qquad \text{Eq (4-1)}$$

Where (ξ, η) are the coordinates of the cross-correlation function. The peak of cross-correlation function, c, is located at $(\xi,\eta)\,|\,c_{\max}$, which will coincide with $(\Delta x,\Delta y)$, locating the position of the peak. This indicates both the magnitude and direction of the displacement between two images.

Giachetti (2000) compared the performance of more than 10 different matching algorithms. It was found that different algorithms have better performance than others under different conditions. Generally speaking, the ZNCC (zero-meaned normalized cross-correlation) algorithm performs the best among the many matching methods.

The matching methods produce a visually attractive flow field. They are also accurate enough for quantitative use. Differential methods are the best when the displacement in the images is small (≤2 pixels), while matching methods work well for moderate displacement. In engineering fields, the matching method is the most used movement estimation method from a sequence of images. Digital image cross-correlation (DIC) is the most commonly used matching method in engineering fields.

4.3.1 Discrete Cross-Correlation

The value of each pixel in the digital image represents a small region in the continuous image being digitized. The cross-correlation function shown in Eq. (4-1) is in the continuous form. In practice, all images have finite dimensions. For two digital images with a relative displacement of (Δm, Δn), $f(m,n)$ and, $g(m,n) = f(m+\Delta m, n+\Delta n)$, with a dimension of M×N, the discrete cross-correlation function is given by:

$$c(l,k) = \sum_{m=1}^{M}\sum_{n=1}^{N} f(m,n)g(m+l,n+k) \qquad \text{Eq (4-2)}$$

Where image matrices, f and g, have the same dimension of M by N.

4.3.2 Zero-meaned Normalized Cross- Correlation

The standard cross-correlation function is shown in Eq. (4-2). When two images cross-correlate with each other, there are some regions out of the correlated area. In the region outside the correlated area, one of the images has to be zero padded in this region in order to get the cross-correlation result.

If the part outside the correlated area is padded by zeros, which is the default method used in most DIC calculations; the cross-correlation function will have a pyramidal shape with its maximum value at the origin.

This will force the correlation peak position toward the origin and introduce a systematic error. Two methods can be applied to reduce this systematic error. The zero-meaned normalized cross-correlation (ZNCC) performs the best among the matching methods (Giachetti 2000), which is used in this research. The discrete form of ZNCC is given as follows.

$$ZNCC(l,k) = \frac{\sum_{m=0}^{M-1}\sum_{n=0}^{N-1}[f(m,n)-\overline{f}][g(m+l,n+k)-\overline{g}]}{\sqrt{\sum_{m=0}^{M-1}\sum_{n=0}^{N-1}[f(m,n)-\overline{f}]^2 \sum_{m=0}^{M-1}\sum_{n=0}^{N-1}[g(m,n)-\overline{g}]^2}} \qquad \text{Eq (4-3)}$$

Where $\overline{f}$ and $\overline{g}$ are the average intensity value of image functions, *f* and *g*.

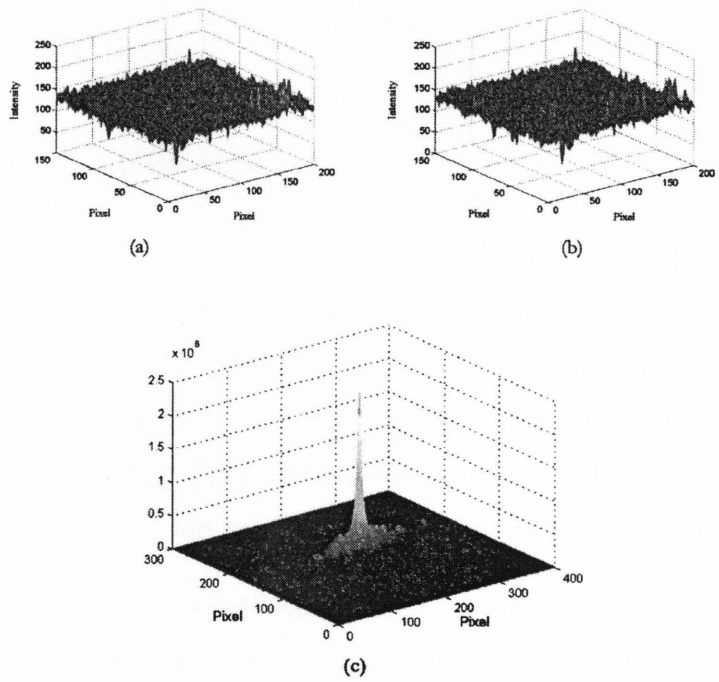

Figure 4.1 Zero-meaned cross-correlation of two images (Liu and Iskander 2003); (a) Image 1, (b) image 2, (c). cross-correlation of images 1 and 2

4.4 HOW DIC WORKS

The peak of auto-correlation function of image 1 (Figure 4.1 a), which is the cross-correlation of image 1 with itself, is at the center of the region, the brightest point (Figure 4.1c). The peak of the cross-correlation of image 1and image 2 (Figure 4.1d) is a small distance away from the center (Figure 4.1c).

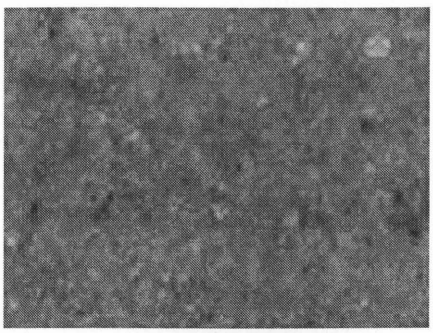

(a) Image 1

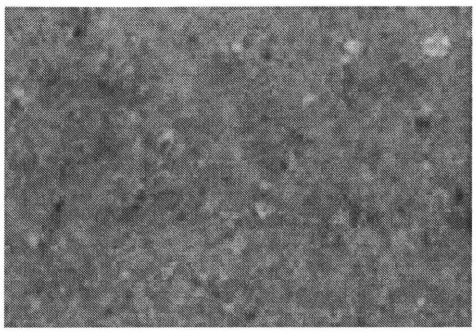

(b) image 2

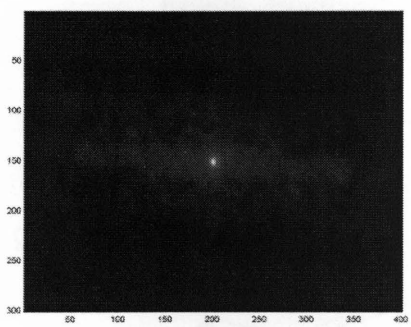

(c) Auto-Correlation

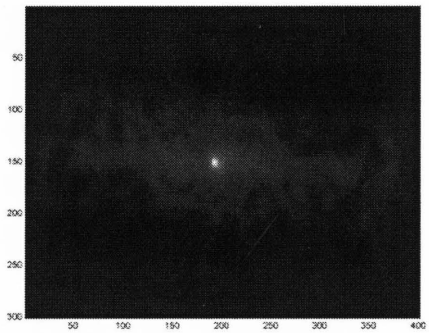

(d) Cross-Correlation Function

Figure 4.2 Normalized Grayscale Images of Correlation Functions (Liu 003)

Figure 4.3 shows the horizontal displacement between the two images. The vector from the center of the region to the peaks of cross-correlation function gives the magnitude and direction of the relative movement between two images.

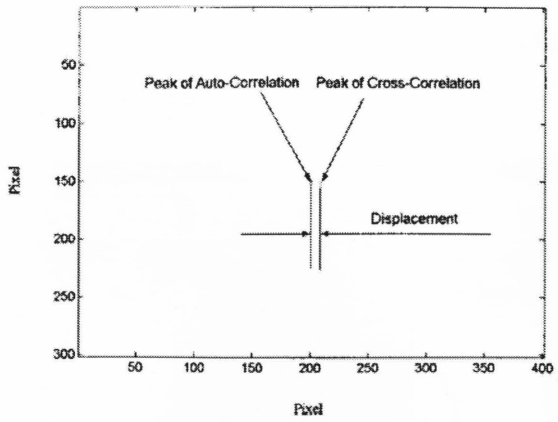

Figure 4.3 The displacement between two images (Liu and Iskander 2003)

The displacement field throughout an image can be obtained by dividing the whole image into small interrogation windows (sub-images) and getting the corresponding movement in each interrogated region.

4.5 PIV SOFTWARE (PIVVIEW)

PIVview is the software used to analyze the captured images of the soil movements around the scaled pile in order to find the displacement pattern. *PIVview* is a compact program package for the evaluation of particle image velocimetry (PIV) or speckle displacement recordings. PIVview was conceived and is maintained by C. Willert, PIVTEC GmbH, Göttingen (Germany), and developed in close cooperation with the PIV-Group of the German Aerospace Center (DLR) in Göttingen.

PIVview is based on single document software architecture, that is, only one image (pair) can be opened by each *PIVview* instance. If it is necessary to open several PIV images simultaneously then the several instances of *PIVview* should be started through the menu option. Once loaded, PIV images are displayed in the main window. Image pairs are displayed by selecting the brightest pixels from both images.

The image (pair) can be interactively interrogated at any position. The interrogation parameters for cross-correlation analysis are defined in various setup menus. The results of the correlation analysis are displayed in the status bar at the bottom as well as in the form of a color-coded vector.

The flow chart of *PIVview* is shown in Figure 4.4, where the whole DIC process is divided into a few steps.

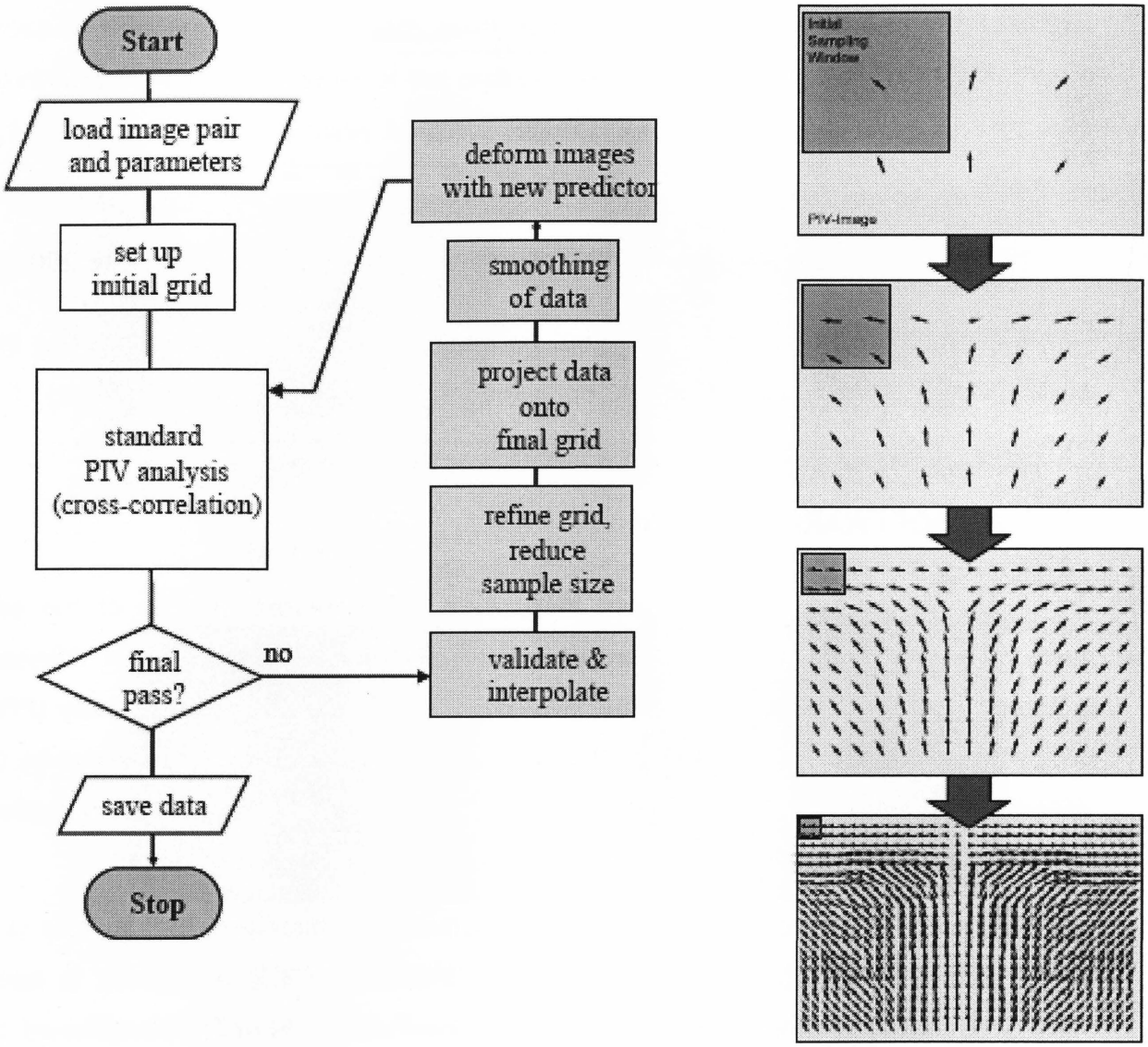

Figure 4.4 Flowchart for coarse-to-fine multi-grid processing with image deformation for second order accurate PIV interrogation

Following are the steps to run the program. First, load a pair of adjacent images to the program, as shown in Figure 4.4. And then choose the appropriate PIV parameters (e.g windows size, grid spacing, correlation properties, filters etc.) as shown in Figures 4.5 – 4.8. Several window sizes used and processed the images as to see which size offers the best results. For all the images, 64x64

produced the best flow patten and it was chosen for the analysis. For all the cases a 50% overlap was applied through a 32x32 grid spacing. Same conditions were used for both horizonal and vertical planes.

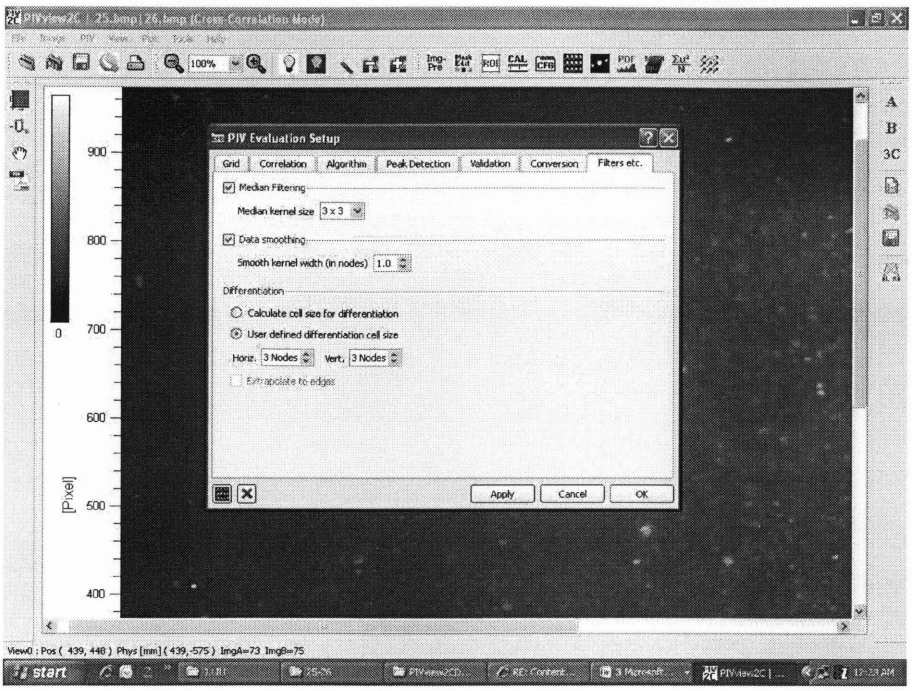

Figure 4.5 Selection menu for PIV parameters

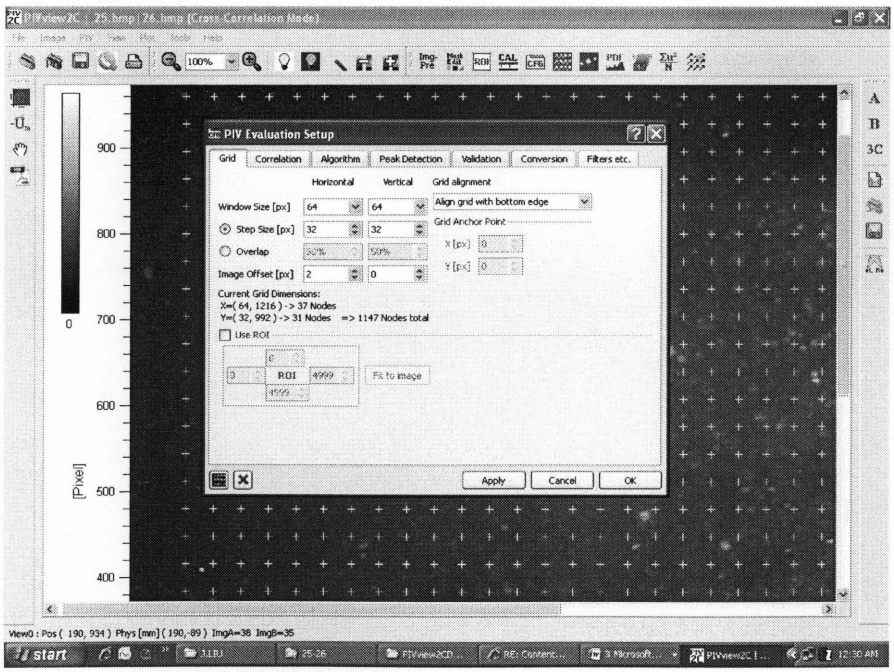

Figure 4.6 Selection menus for the window size and grid spacing

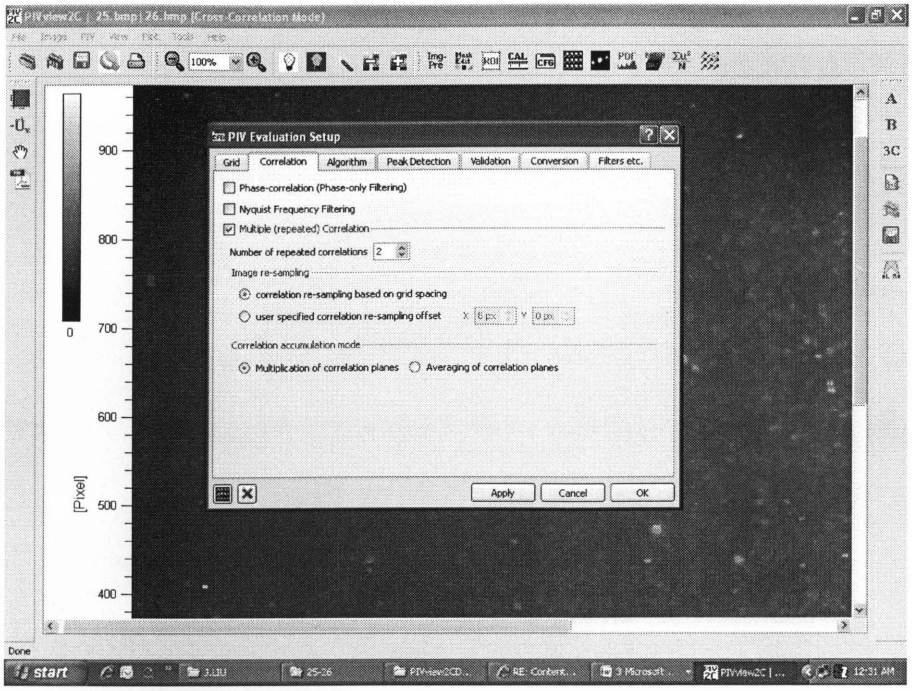

Figure 4.7 Selection menus for the correlation properties

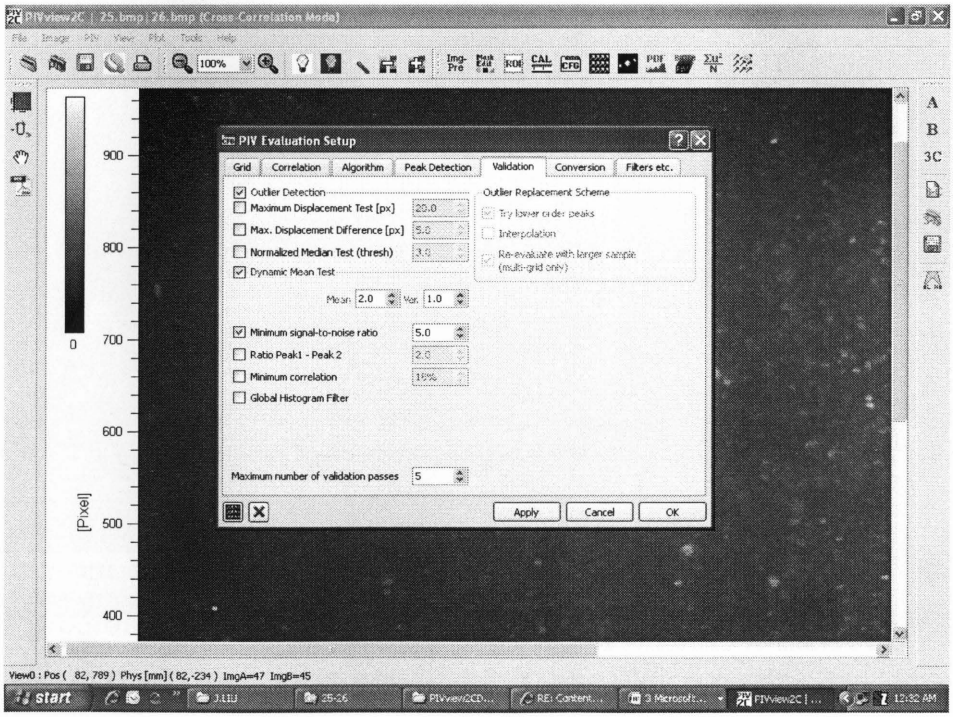

Figure 4.8 Selection menus for filters

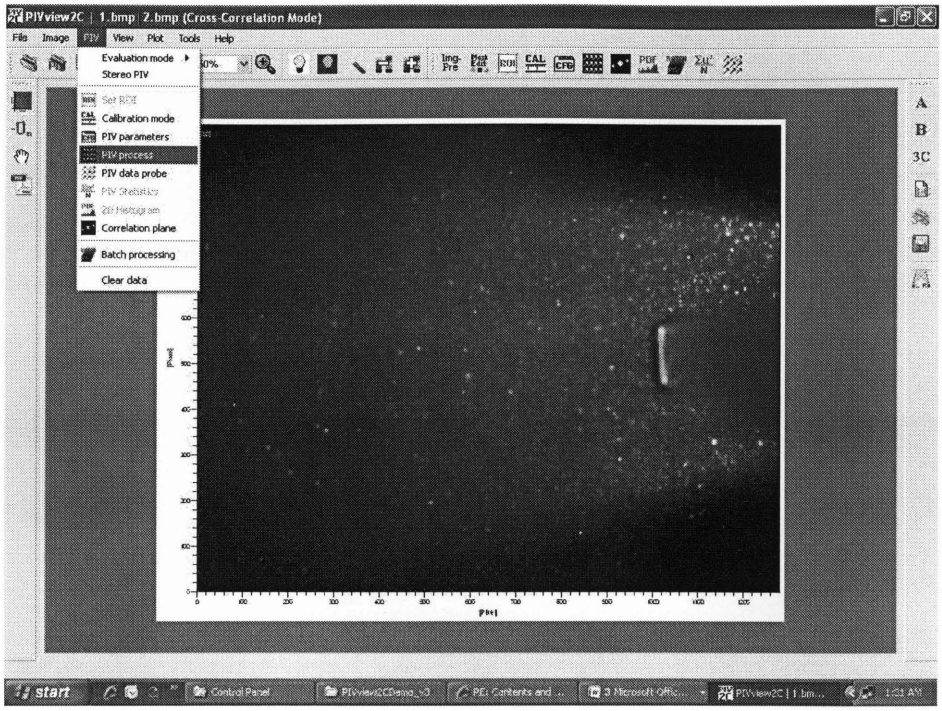

Figure 4.9 Processing window

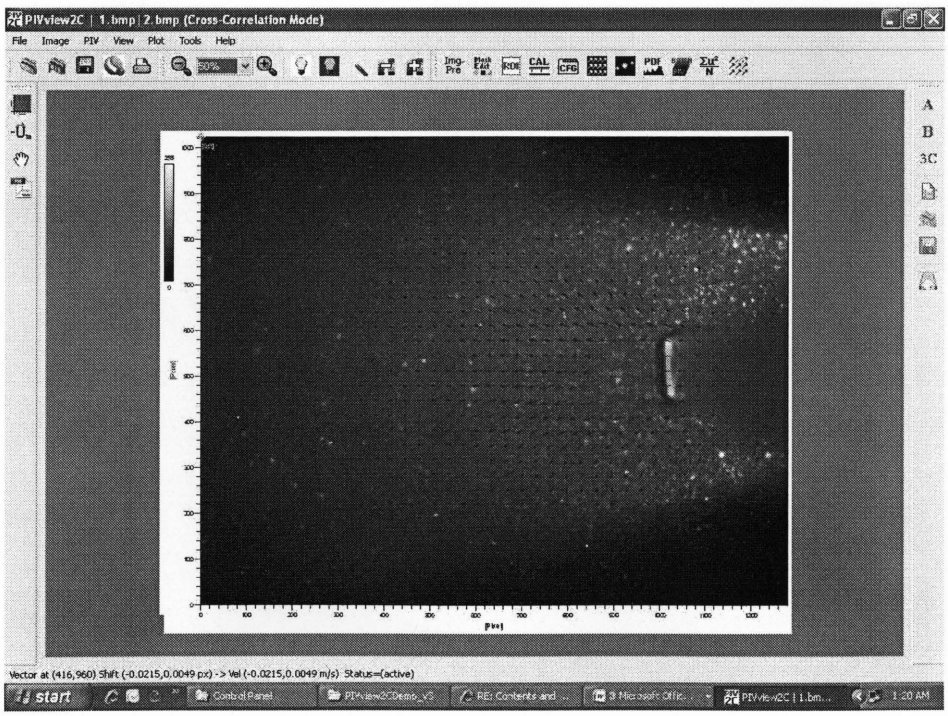

Figure 4.10 Deformation pattern

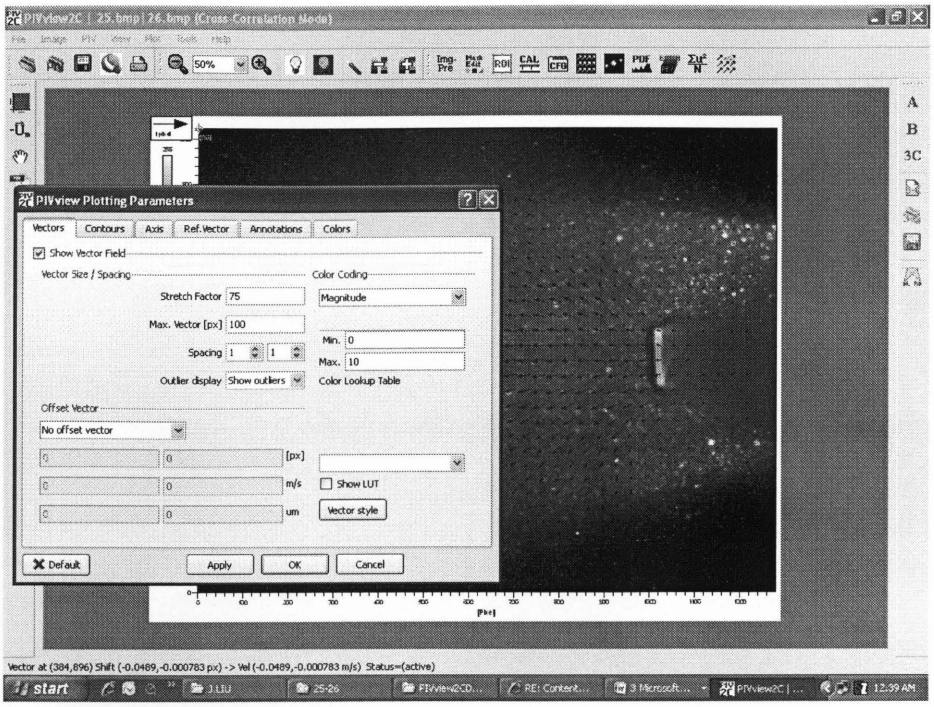

Figure 4.11 Selection menu for plotting (with the background)

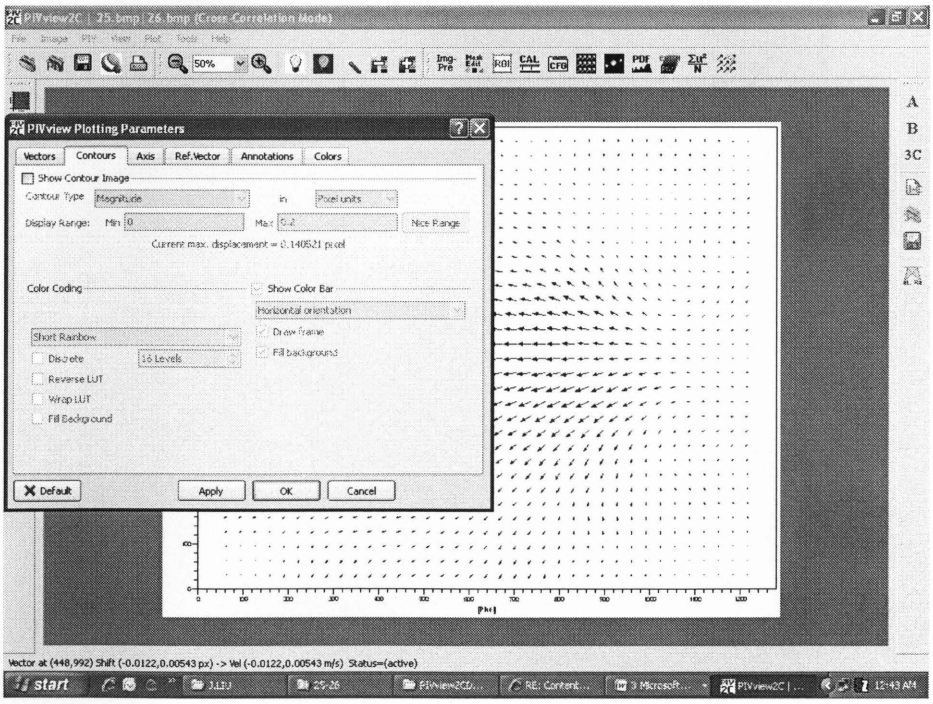

Figure 4.12 Selection menus for plotting (without background)

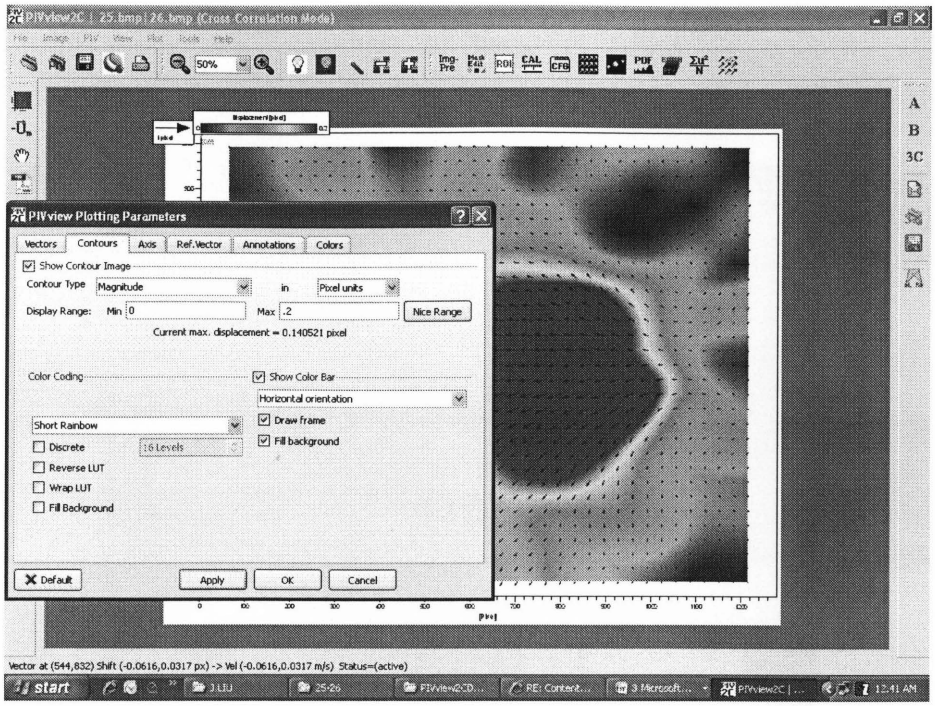

Figure 4.13 Selection menus for plotting (displacement contour)

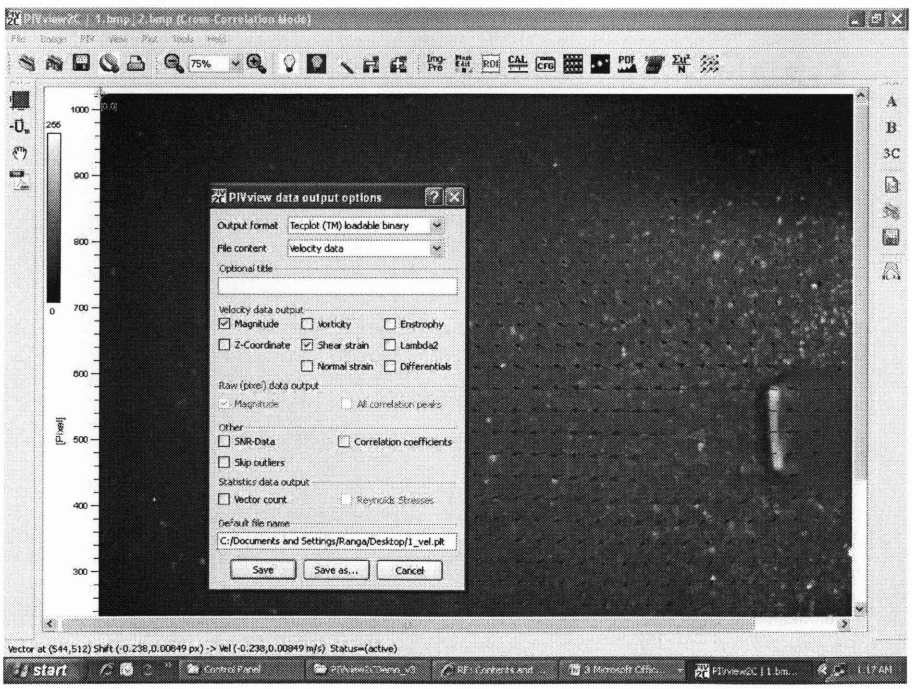

Figure 4.14 Saving data in velocity form (shear)

When the image processing is completed, the data files are saved in two formats; one has the dispacement while the other carries the shear information. Teckplot (graphic software) is used to generate the shear contours and the displacement contours.

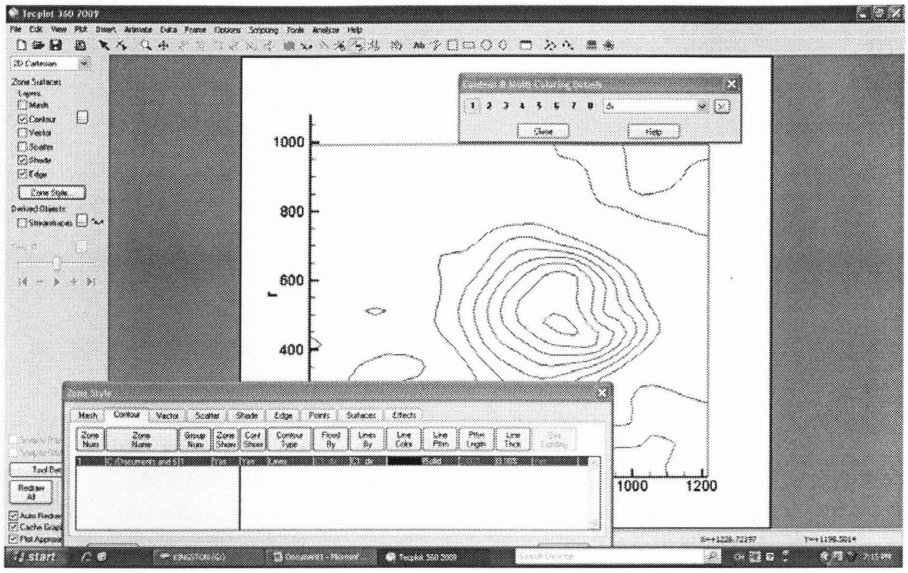

Figure 4.15 Displacements contour lines (output by Tecplot)

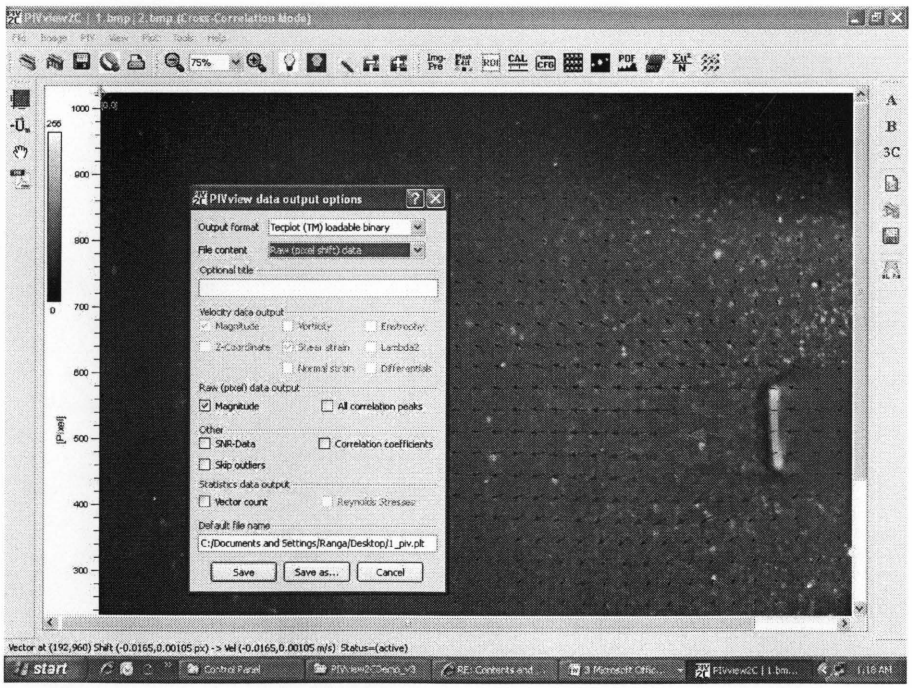

Figure 4.16 Saving data in terms of pixel movements

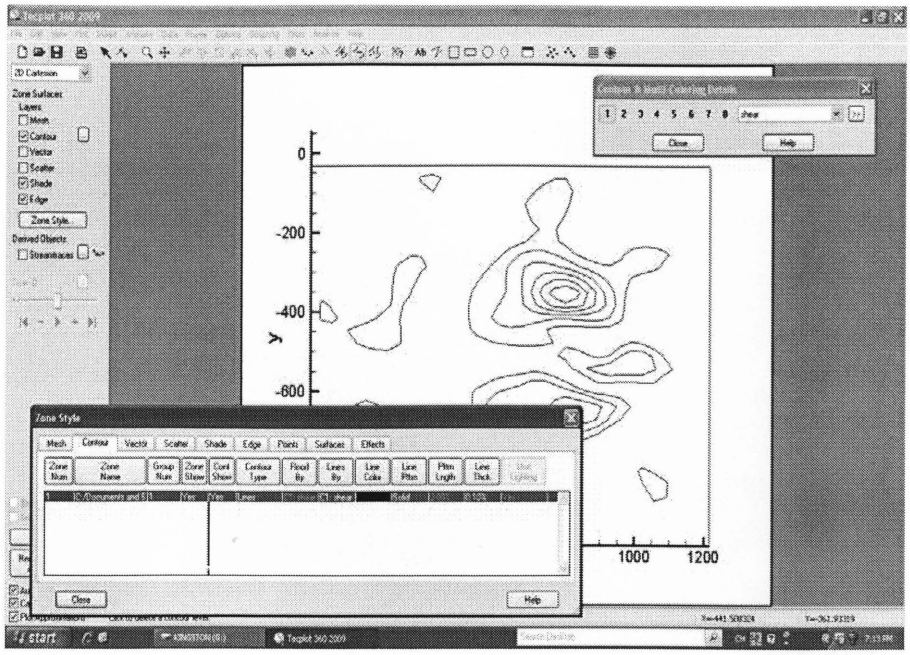

Figure 4.17 Shear contour (output by Tecplot)

CHAPTER 5

EXPERIMENTAL SETUP AND TEST PROCEDURE

5.1 EXPERIMENTAL SETUP

A test set-up is developed in this research, which consists of a PixeLink (PL-B741E) mono complimentary metal-oxide semiconductor (CMOS) camera , a laser light source, a line generator lens, a loading frame, a test table, and a PC for image processing, as schematically shown in Figure 5.1. The camera has a resolution of 1280 x 1024 pixels. It is controlled by the PC through PixeLINK Capture OEM software. The camera is positioned accordingly to capture the images in both the vertical and horizontal planes. A high power Laser system made by JDS Uniphase (model-1145AP-3340), with an output power of 35 mW, is used to provide a powerful laser beam. The line generator lens is utilized to create a laser sheet from the laser beam in order to slice the sample. The lateral loading arrangement consists of a string, a load cell (capacity - 20 lbs) attached to a LVDT (with a linear strike of ±1 inch). A data acquisition system is used to measure the applied horizontal load and the displacement of the scaled acrylic pile driven to the transparent soil model housed in a Plexiglas mould. The actual test set-up is shown in Figure 5.2.

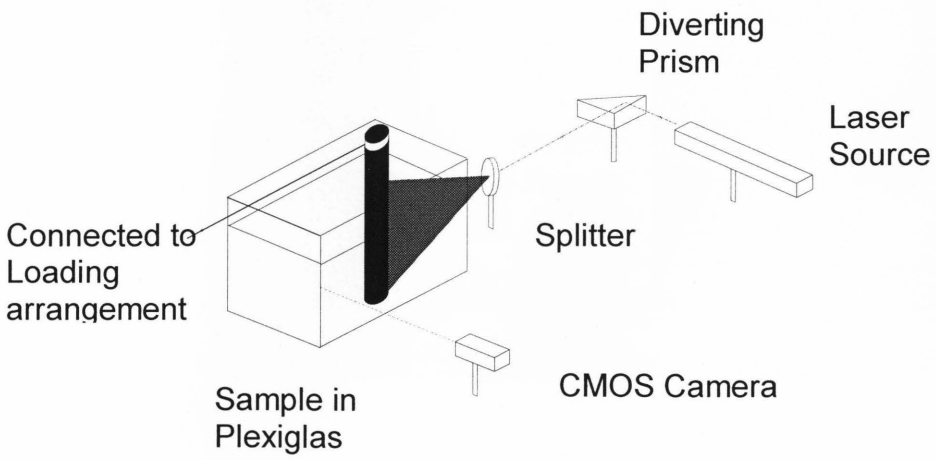

Figure 5.1 Schematic diagram of the experiment setup

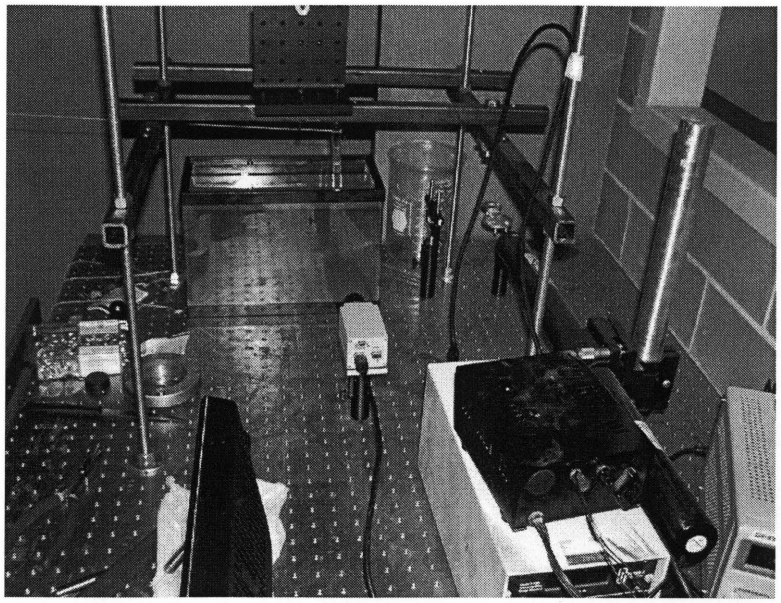

Figure 5.2 The experiment setup

5.2 SAMPLE PREPARATION

The transparent soil model shown in Figure 5.3 was prepared by mixing fine silica gels with the pore fluid (50:50 blend of mineral oil and solvent). The mix was de-aired using a vacuum container. The sample was made in small quantities to make the de-airing process easy and effective. Once the required amount (8 Lt) was prepared, all the small samples were transferred to a Plexiglas mould carefully not to create any air bubbles using a table spoon.

Figure 5.3 Transparency of transparent soil sample

5.2.1 Transparent Soil Model

The transparent soil sample was housed in a Plexiglas mould of 30 cm length, 15 cm width and 20 cm height. The model width is limited by the depth of penetration of the laser beam. Based on the power of this laser, the penetration depth can go up to 15 cm into the sample. The model thickness is limited by transparency degradation due to imperfect matching of the refractive indices of the solid particles and the pore fluid and impurity of the sample particle itself.

5.2.2 Laser Beam

The laser beam used in this research is a high power Laser system made by JDS Uniphase (model-1145AP-3340), with an output power of 35 mW. The diameter of the laser beam is approximately 1 mm.

5.2.3 Line Generator Lens

A line generator lens is used for generating the laser sheet. The line generator is a cylindrical lens that expands the laser beam in one direction only. It has to be set in two different positions to generate both vertical and horizontal laser sheets.

5.2.4 CMOS Camera (complimentary metal-oxide semiconductor)

The camera used in this research was a PixeLink (PL-B741E) made by PixeLINK (3030 Conroy Road, Ottawa, ON K1G 6C2). It has the following technical specifications;

Resolution	1.3 MP, 1280(H) x 1024(V)
Pixel Pitch	6.7 μm x 6.7 μm
Active Area	8.57 mm x 6.86 mm - 11.01 mm diagonal

Though still cameras can give high resolutions, the main disadvantage is that downloading the images requires stopping the experiment and connecting the camera to a PC. Comparatively priced industrial CMOS cameras offer a lower resolution but more convenience. PixeLINK Capture OEM was free downloaded from www.pixelink.com for capturing the images.

Zoom is applied digitally in many digital cameras. The speckle information is lost if a digital zoom is used and, consequently, particle movement information is lost; therefore, a digital zoom cannot be used. Also, images have to be stored in a non-lossy format, such as TIFF or BMP, to prevent loss of information during compression.

5.2.5 Loading Arrangement

A modified component from an apparatus which has a horizontally movable head with a rotary arm was used as the loading frame. The loading cell with a capacity of 20 lbs was mounted on the head as shown in the Figure 5.4 and the LVDT was attached at the back. Both the loading and the displacement signals were monitored with a PC through a data acquisition system programmed using *Labview*. The horizontal string connected to the model pile was attached to load cell and the sagging of the string was adjusted. With the rotation of the rotary arm the pile was loaded horizontally and the readings from both the loading cell and the LVDT were acquired and stored in the computer.

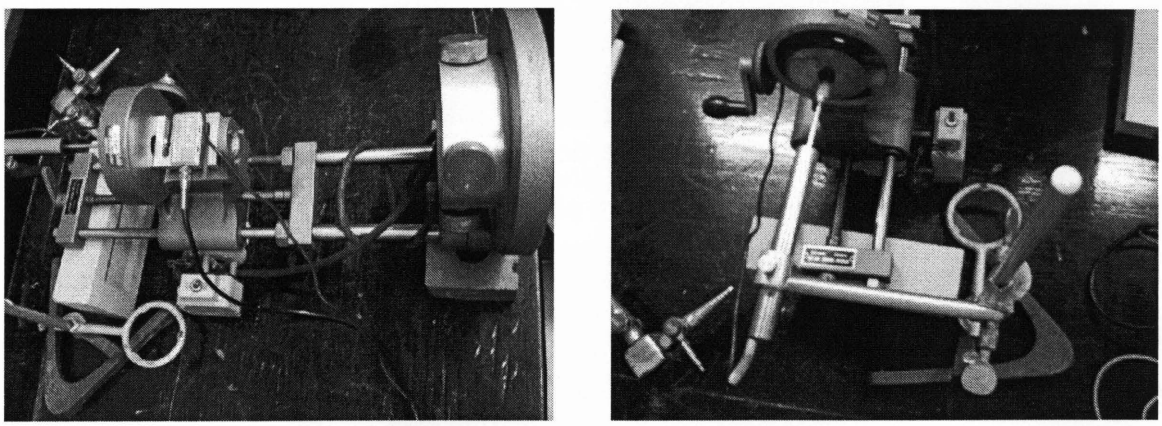

Figure 5.4 Loading arrangement

5.3 TEST PROCEDURE

The sample was positioned on the test table and the model pile was driven into the soil. The pile was connected to the loading arrangement (Figure 5.4) using a horizontal string to provide the lateral load and the LVDT was adjusted accordingly.

Once the setup was complete, a laser light sheet was sent through the line generator lens using the laser source and the CMOS camera positioned accordingly for capturing images in both vertical and horizontal planes. The camera was focused looking through the computer screen. After that the pile was applied a gradually increasing horizontal load with the loading arrangement.

The camera was program controlled through an in-house developed software using *MATLAB* to capture the images through the cameras and store the images in a temporary folder in the computer during the testing. These images were downloaded from the temporary folder for later image processing. Another data acquisition system programmed by *Labview* recorded the applied load and the horizontal deflection simultaneously. These data was transferred to computer later to obtain the load-displacement curve of each test condition.

Three different pile geometries (round, solid- square, hollow -square) were used to observe the different soil movements due to the shape. The sample was sliced in both horizontal and vertical directions to visualize the soil displacement due to the horizontal loading on both planes.

5.4 OPTICAL SETUP CALIBRATION

Calibration is a validation process of specific measurement techniques and equipment. In this research, calibration is done to correlate the displacement from optical measurement to the displacement in physical space.

Before the actual test was performed, the optical setup was calibrated using a small sample, the camera, and a linear stage. The sample was mounted on the linear stage and sliced horizontally with a laser sheet. An image was taken in this position. Then the sample was moved horizontally through a distance of 0.25 inch (6.35 mm) and a second image was taken in this position.

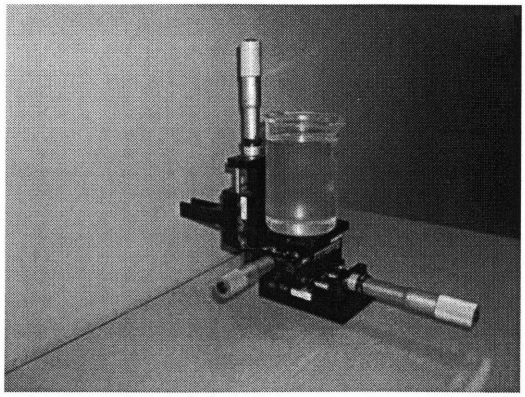

Figure 5.5 The sample mounted on the linear stage for calibration

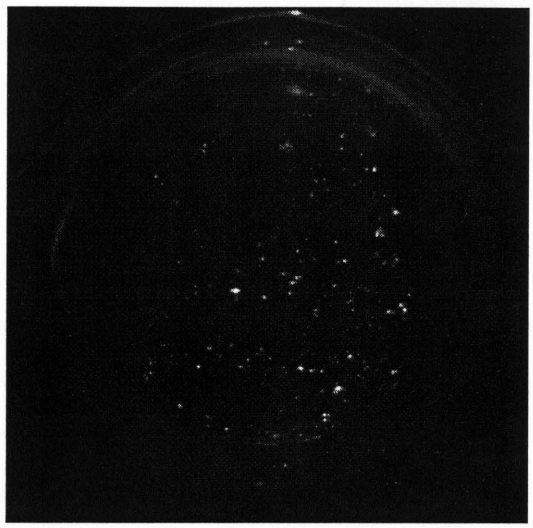

Figure 5.6 Image of the horizontally sliced sample during calibration

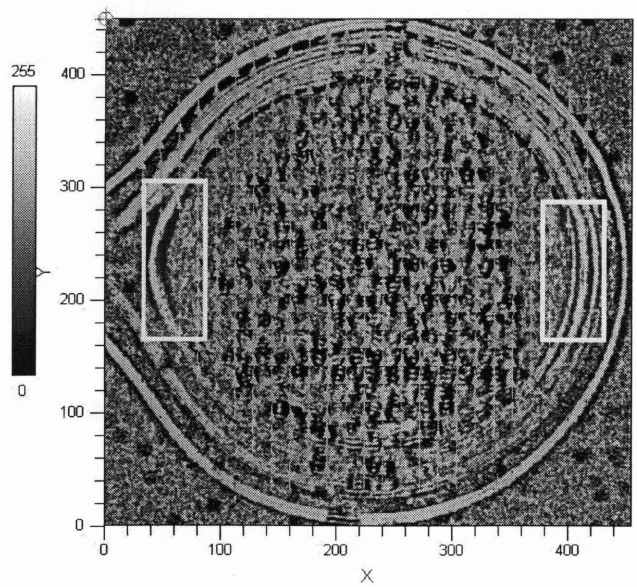

Figure 5.7 PIVview image for the calibration of the optical system

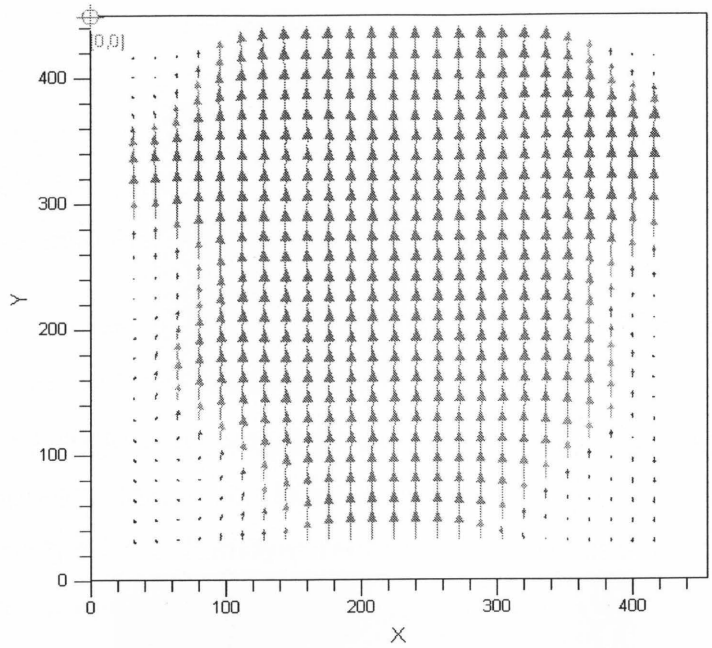

Figure 5.8 Displacement pattern of the sample during calibration (PIVview)

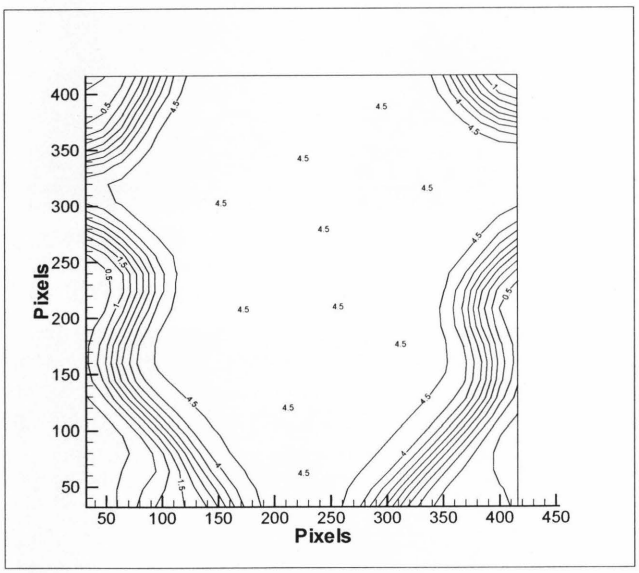

Figure 5.9 Displacement contour of the sample (PIVview)

The particles in the area marked with the rectangles (Figure 5.7) have not displayed the expected movement due to the diverging pattern of the laser sheet, and the corresponding contour pattern is shown in Figure 5.9

$$\text{Optical Scale} = \frac{\text{Actual displacement (mm)}}{\text{Optical displacement pixel)}}$$

Actual displacement of the sample = 6.35 mm

Optical displacement (Figure 4.a) = 4.5 pixel

Optical scale = 1.411 (mm/pixel)

5.4 CONCLUSIONS

A test set-up was developed specifically for this research, which consisted of a Mono CMOS camera, a laser light source, a line generator lens, a loading frame (with a load cell and a LVDT), a test table, and a PC for image processing. The camera was controlled by the PC through a *MATLAB* software. The load cell and the LVDT were controlled by a Labview software to acquire data during capturing images. In the future, the test set-up can be updated with the camera control and the load cell and LVDT control developed within the same software environment. At the same time, the synchronization of data acquisition with image capturing to avoid errors in identifying corresponding load and deformation information with images.

CHAPTER 6

DATA ANALYSES AND RESULTS

6.1 INTRODUCTION

The main purpose of this research is to visualize an internal soil (sand) deformation field around a laterally loaded vertical pile. In order to understand the deformation pattern changes related to the pile geometry, two different shaped piles were used in the tests: a cubic pile and a cylindrical pile. In order to see the influence of pile stiffness on the deformation and load capacity, two cubic piles are used in this study: a solid cubic pile and a hollow cubic pile. The three model piles were made of acrylic and had a diameter or width of 12.7 mm. During the tests, a series of pictures were taken with the CMOS camera to capture the movement of surrounding soil during the test while the pile was being applied a horizontal load. The images were automatically transferred and saved in the computer for later image processing. The test was done for both horizontal and vertical planes and the test components were adjusted accordingly. The images were processed with PIVview software.

6.2 SOIL MOVEMENT AROUND A SOLID CYLINDRICAL PILE

Figure 6.1 shows the relationship between the applied horizontal load and the lateral deflection of the solid round pile at the loading point during the test. The loading point is about 3 cm above the soil surface. This is the same load exerted on the pile by the surrounding soil. The initial portion of the curve is straight (approximately) and after that the gradient is varying. This reflects the non-linear behavior of real soil and the shape of the graph is very much similar to that of loose fine sand. Therefore, the transparent soil used in this experiment is a good representative for the real soil and can get a better understanding about the unseen internal soil movements.

It is worthy of note that there is a heavy fluctuation in the figure especially

post-peak load stages. It is believed that, the high compressibility of silica gel due to a two-pore system inside contributes to this phenomenon. The breakage of silica gel may also contribute to the fluctuation.

Figure 6.2 shows two consecutive images taken at the loading stage A, during the test. The speckles in the images are from the interaction between laser light and transparent soil. In this research the soil movement is measured by tracking the changes of these speckles. When these two pictures are processed with PIVview software as described in chapter 4, it reveals soil movement due to the relative movement in the pile. For example, the Figure 6.3 shows the displacement pattern of soil.

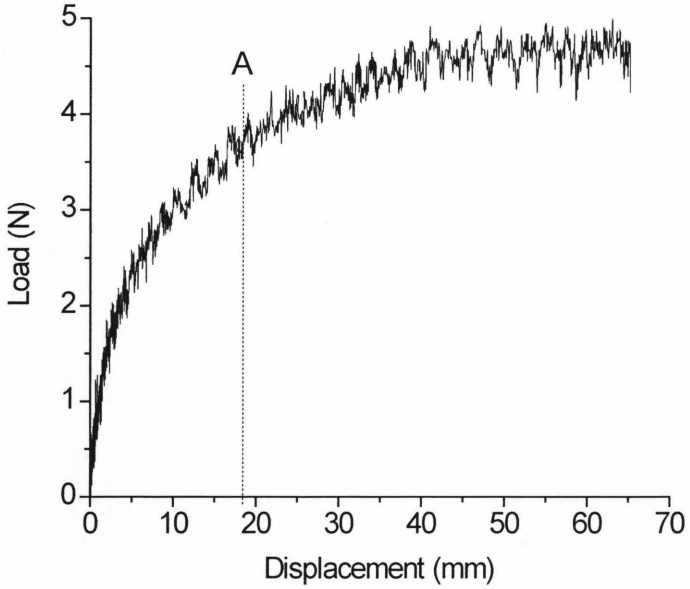

Figure 6.1 The Load vs. displacement curve for a solid round pile

The arrow patterns are not very clear due to insertion of the actual image in the background and it can be clearly seen in Figure 6.4 where a blank background is used. In order to visualize the intensity of deformation in the soil, contours can be used as shown in two different conditions: shaded contour image (Figure. 6.5) and line contour image (Figure. 6.6). The deformation of soil inside transparent soil shows the typical soil

behavior explained in chapter 2. It further presents the facts that transparent soil can be used to model natural soil.

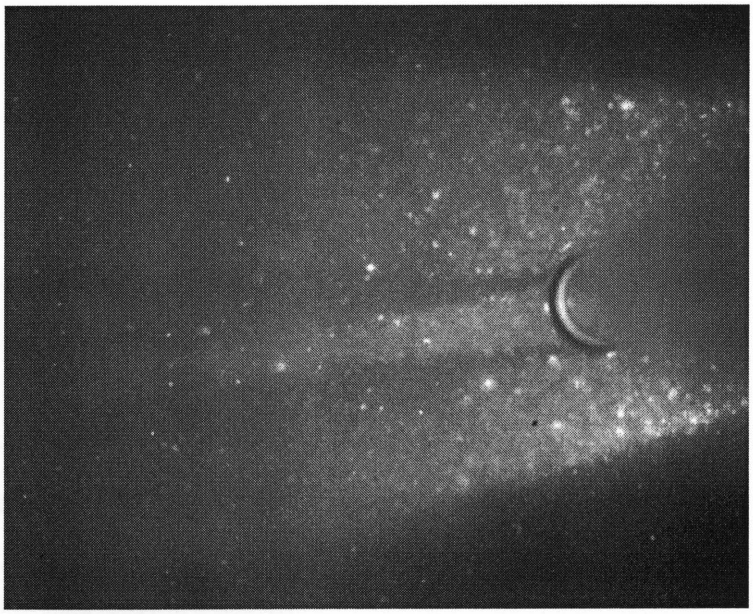

a) the first image before a relative movement in the pile

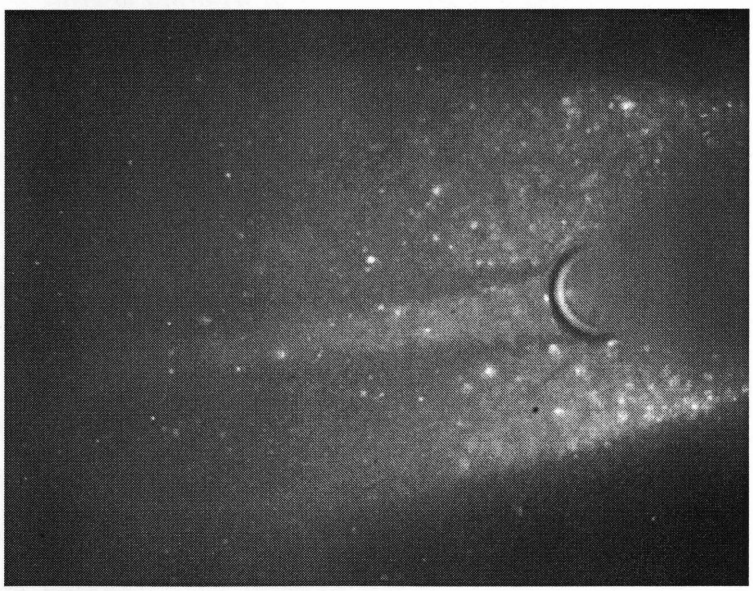

b) the second image after a relative movement in the pile

Figure 6.2 Two consecutive images before and after a movement in the pile (stage A)

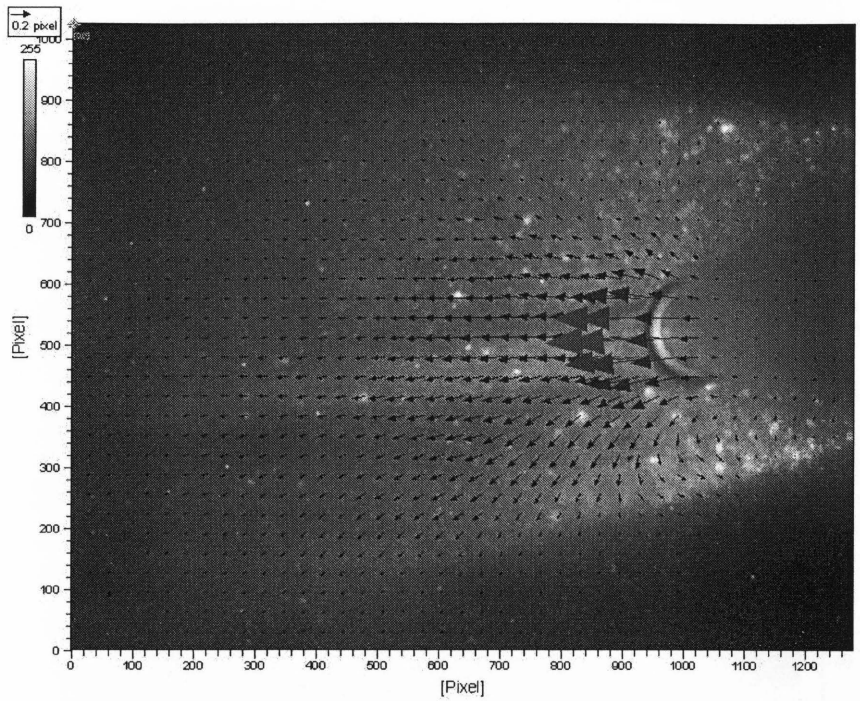

Figure 6.3 Soil deformation pattern (pile image inserted as the background)

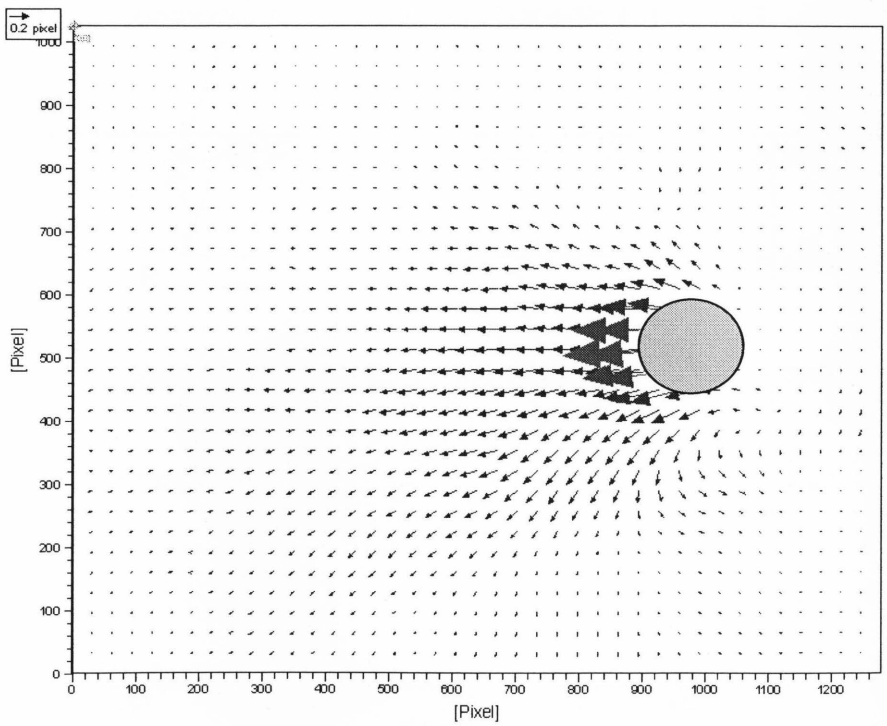

Figure 6.4 Soil deformation pattern (without the actual background)

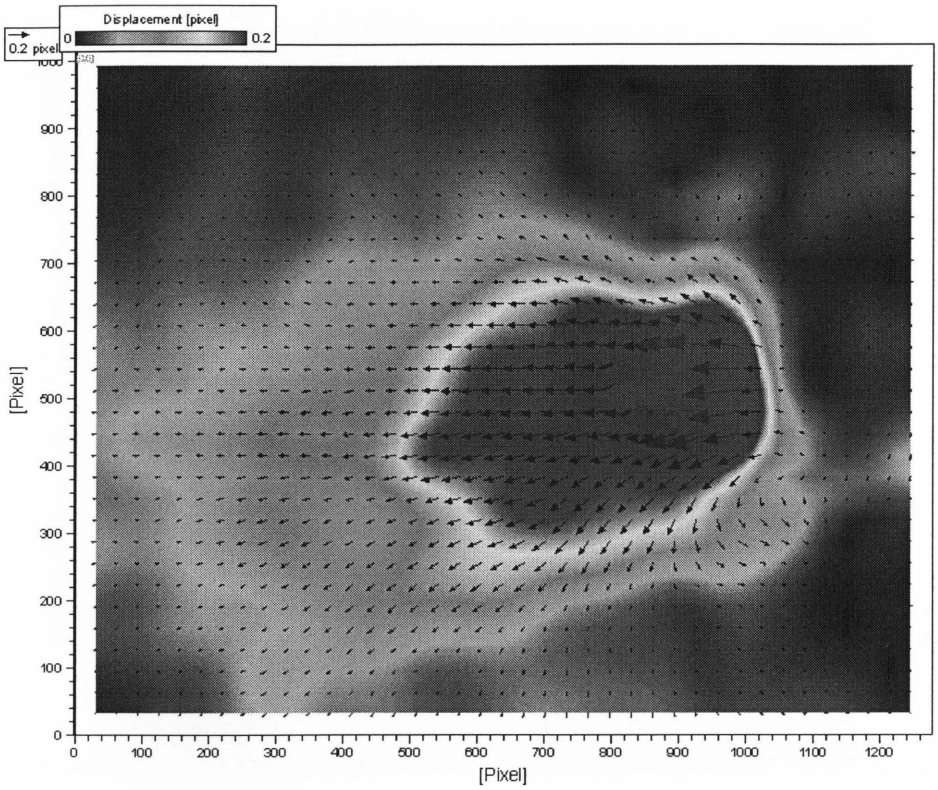

Figure 6.5 Shaded soil displacement contour

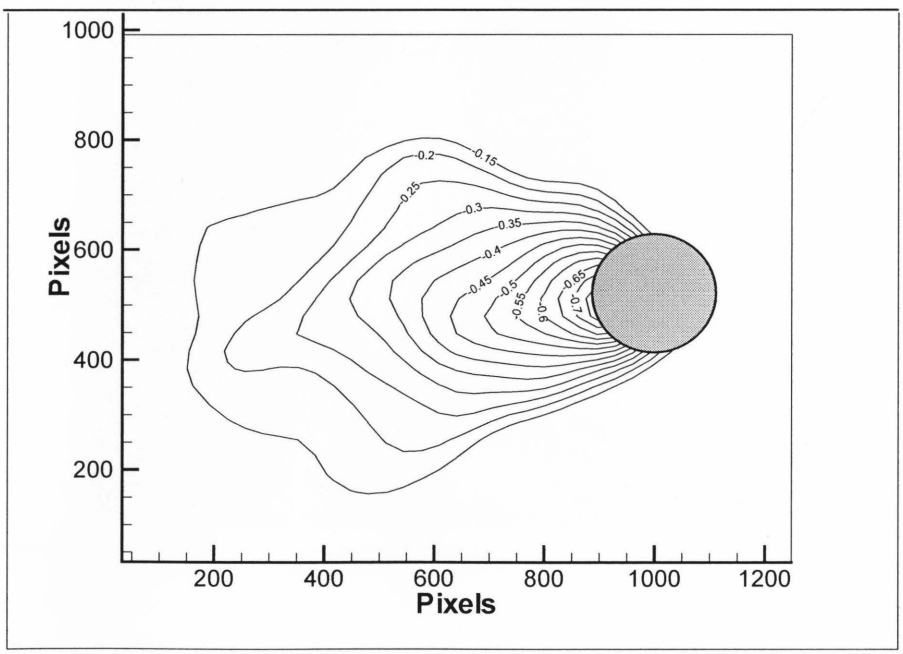

Figure 6.6 Displacement contour lines

The strains can be deduced from the displacements. The failure plane can be studied by the maximum shear strain, since soil is normally assumed to fail due to shearing stress. Figure 6.7 shows the shear strain contour of transparent soil. It can be the failure plane, which is curved outward from the pile edge. This pattern is similar to that natural soil. However, the straight line is normally used in practice because of its simple shape. It is worthy of note that the extension of the failure plane cannot be identified only from the results for the horizontal plane.

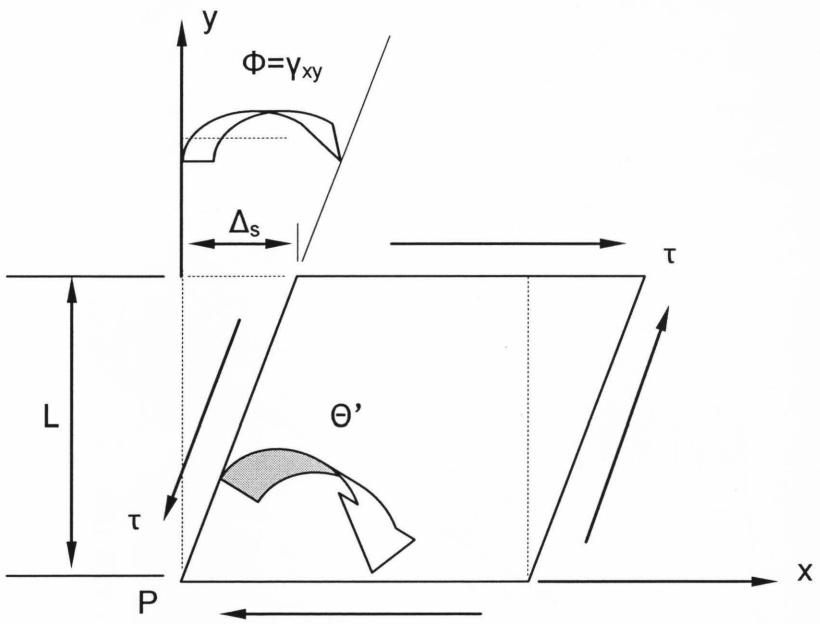

Figure 6.7 Shear Strain (γ) Element

$$\gamma_{avg} = \frac{\Delta_s}{L_s} = \tan\phi \qquad \text{Eq (6-1)}$$

$$\gamma_{xy}(P) = \frac{d\Delta_s}{dL_s} \qquad \text{Eq (6-2)}$$

$$\gamma_{xy}(P) = \frac{\pi}{2} - \theta' \qquad \text{Eq (6-3)}$$

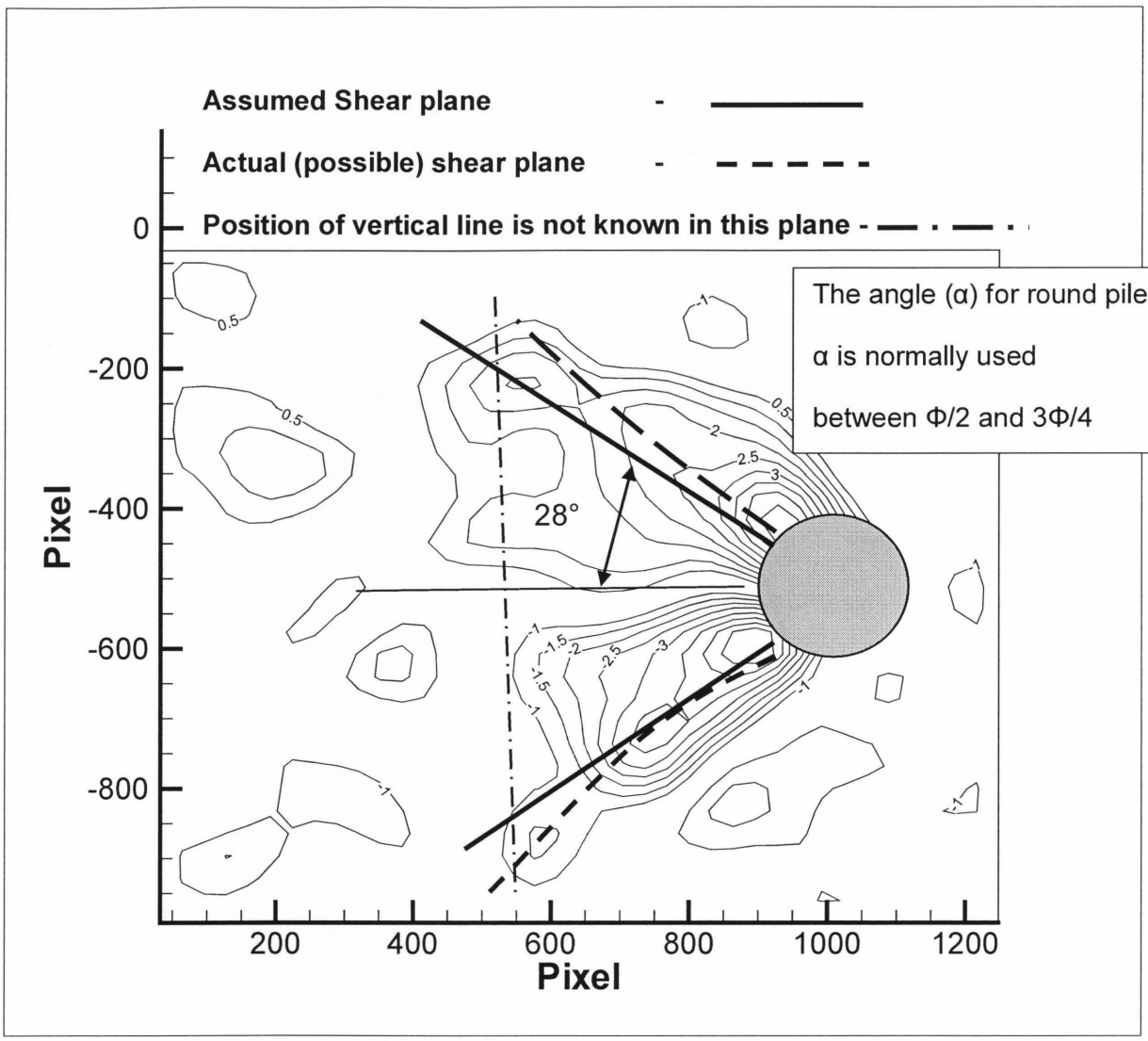

Figure 6.8 Shear strain contours and potential failure plane

6.3 SOIL MOVEMENT AROUND A HOLLOW CUBICAL PILE

The same procedure was followed for a hollow square shaped pile. Figure 6.9 shows the load vs. displacement curve of the pile at the loading point. The loading point is approximately 3 cm above soil surface. Normally it is expected to have higher loading capacity from a cubical pile compared to a cylindrical pile of the same diameter. However the load from the cubical pile is smaller than the cylindrical pile. It is believed the testing procedure and depth difference in two tests contributed to this discrepancy. The horizontal round shape pile was the first test done using the soil sample. During the pile replacement for the second test for a cubical pile, the soil was mobilized and disturbed and the soil pile interaction may be very different from the first one. In the future tests, it is recommended to standardize the sample preparation to provide a better comparison.

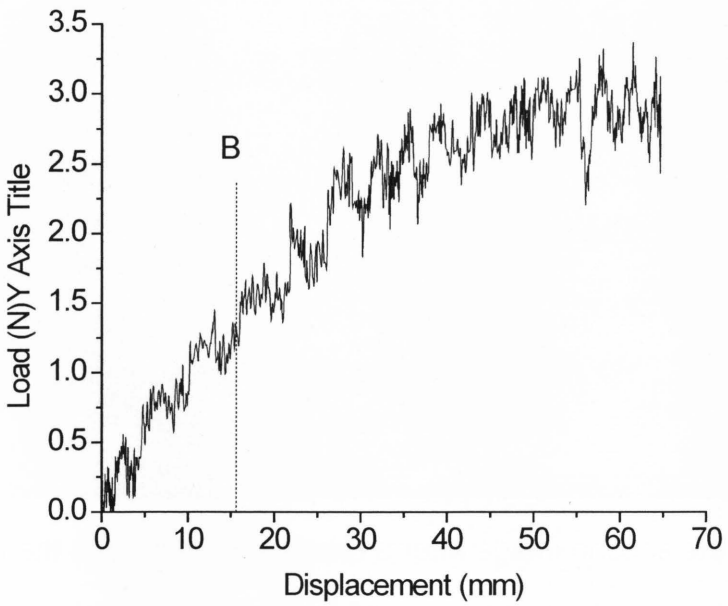

Figure 6.9 Load vs. displacement curve for a hollow square pile

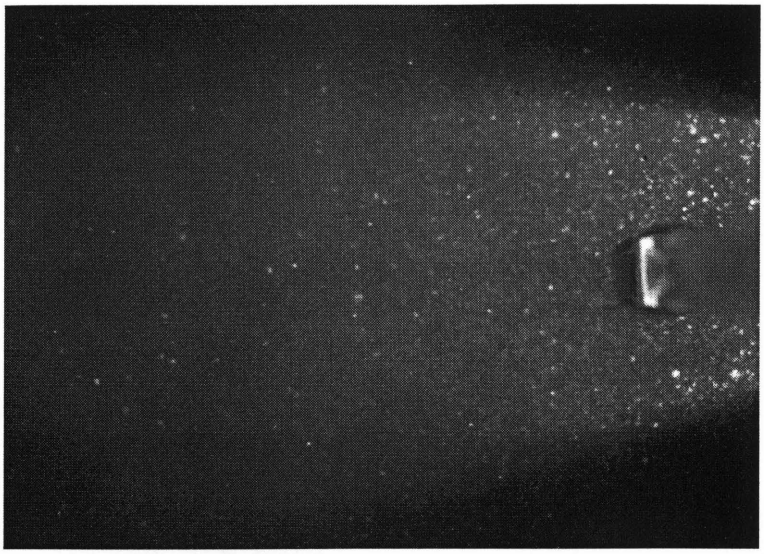

a) the first image before a relative movement in the pile

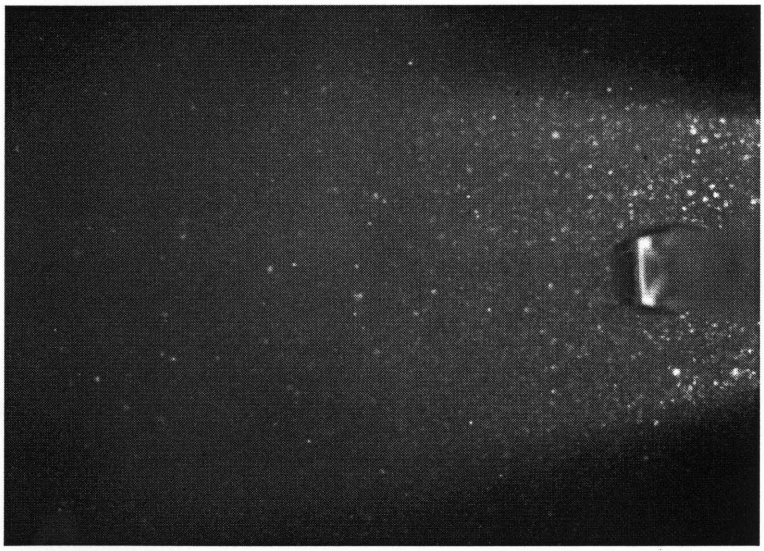

b) the second image after a relative movement in the pile

Figure 6.10 Two consecutive images before and after a movement in the pile (stage B)

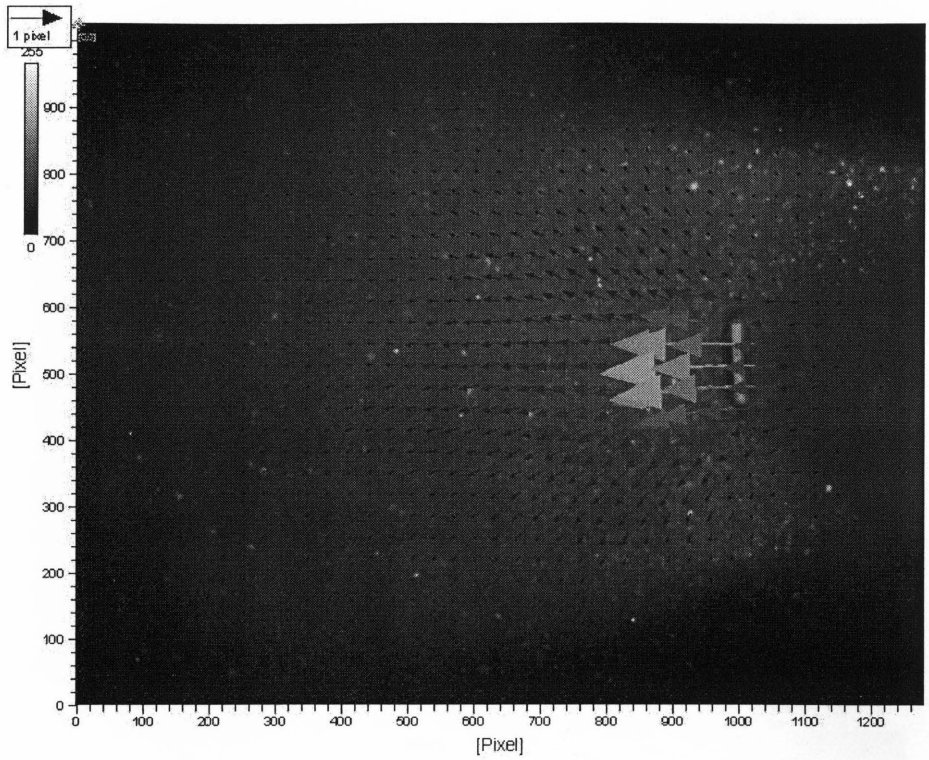

Figure 6.11 Soil deformation pattern (pile image inserted as the background)

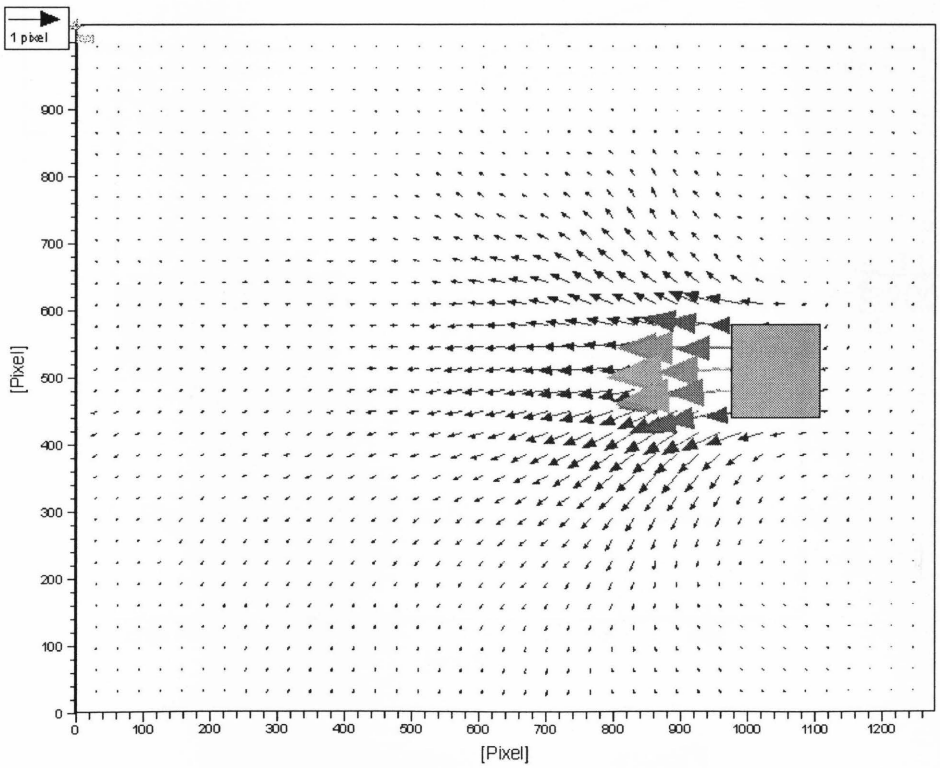

Figure 6.12 Deformation pattern (without the actual background)

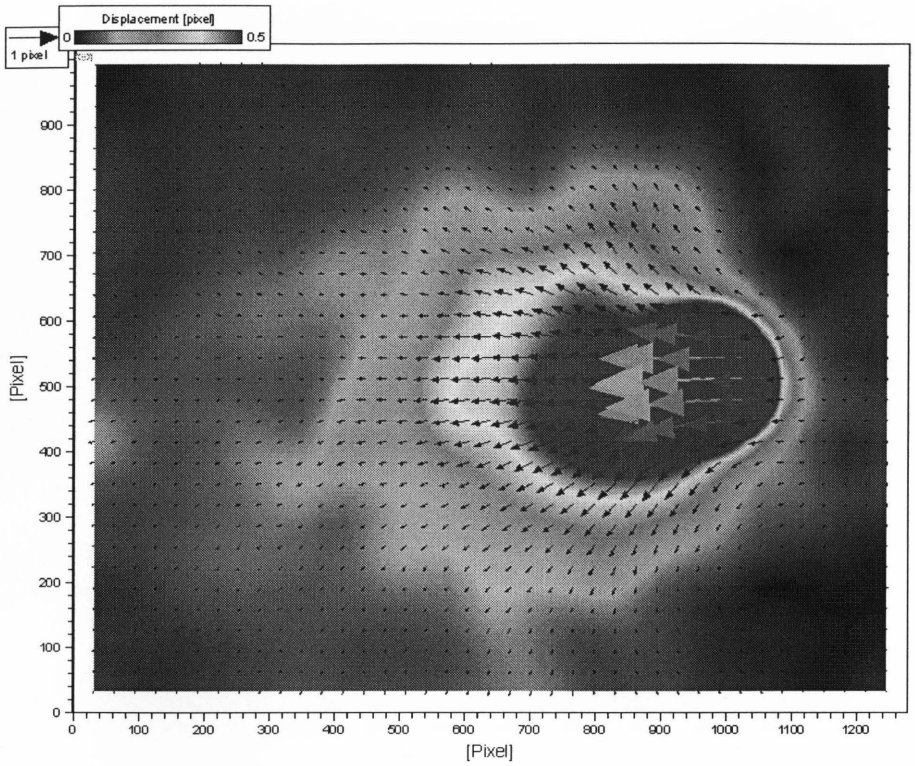

Figure 6.13 Shaded displacement contour

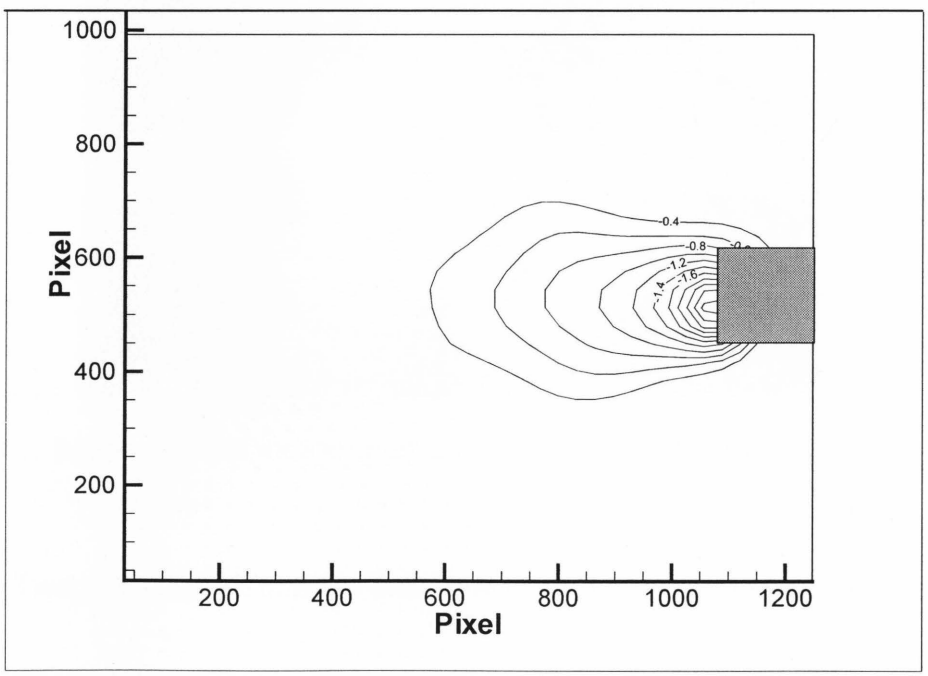

Figure 6.14 Displacement contour

A similar phenomenon can be found in the strain field, as shown in Figure 6.14, where the failure plane is a curve.

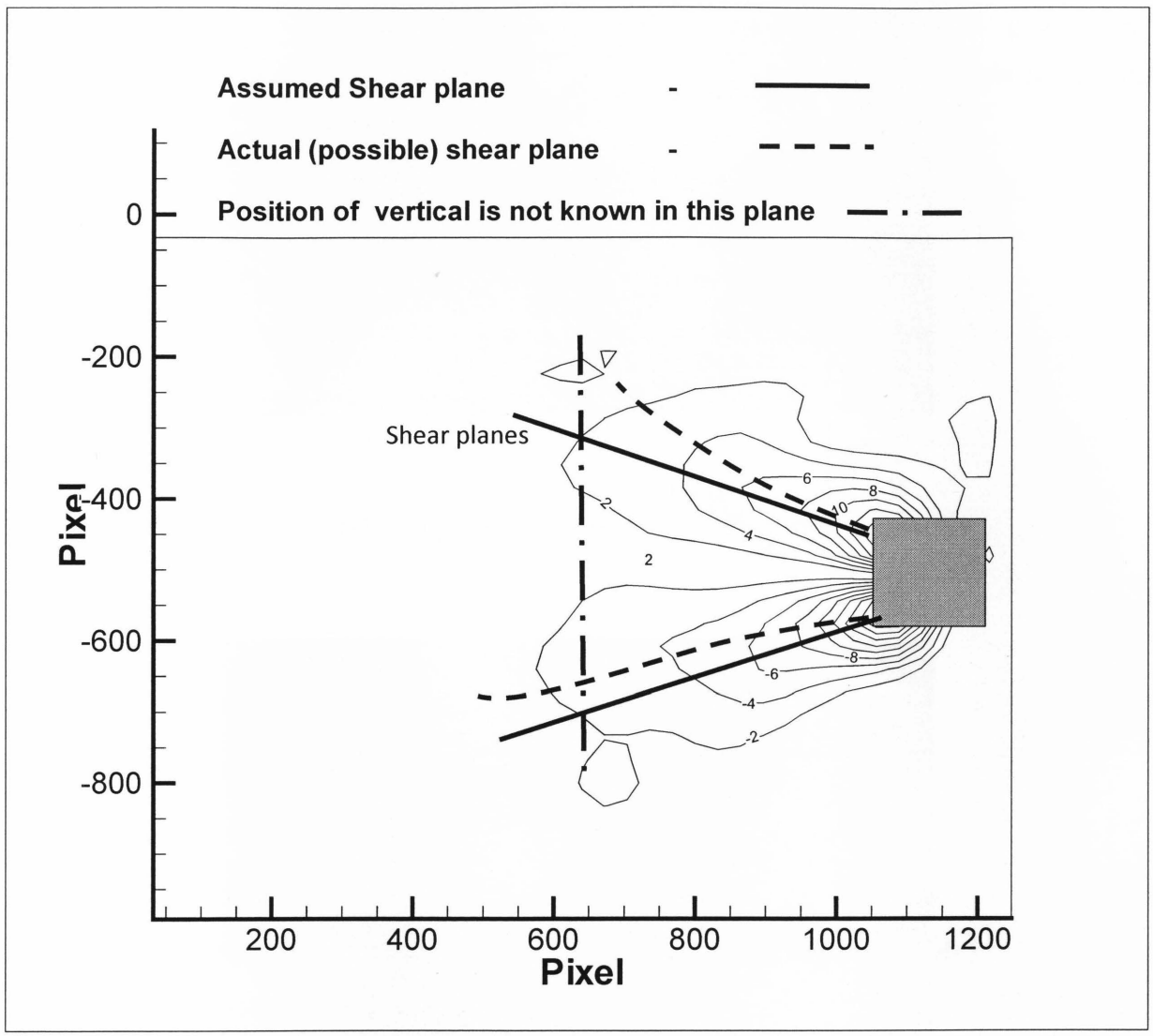

Figure 6.15 Shear contours and potential failure plane

6.4 SOIL MOVEMENT AROUND A SOLID CUBICAL PILE

As expected, the load capacity of solid cubic pile is much higher than a hollow cubical pile, as shown in Figure 6.15. Compared to Figure 6.9 for a hollow cubical pile, the loading capacity at the peak loading stage increased from about 2.75 N to approximately 4.5 N in a solid pile case.

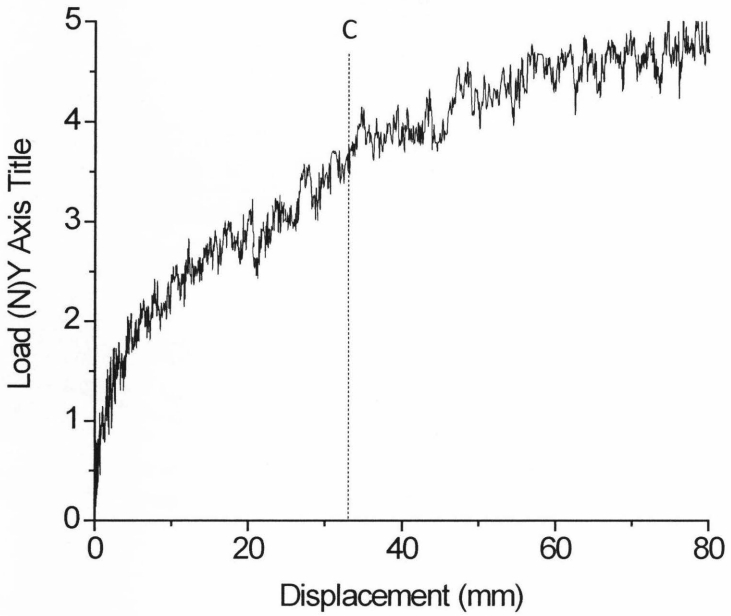

Figure 6.16 Load vs. displacement curve for a solid square pile

Following the same procedure, the displacement field and strain field were obtained based on image processing method. The results are shown in Figure 6. 18 - Figure 6.20.

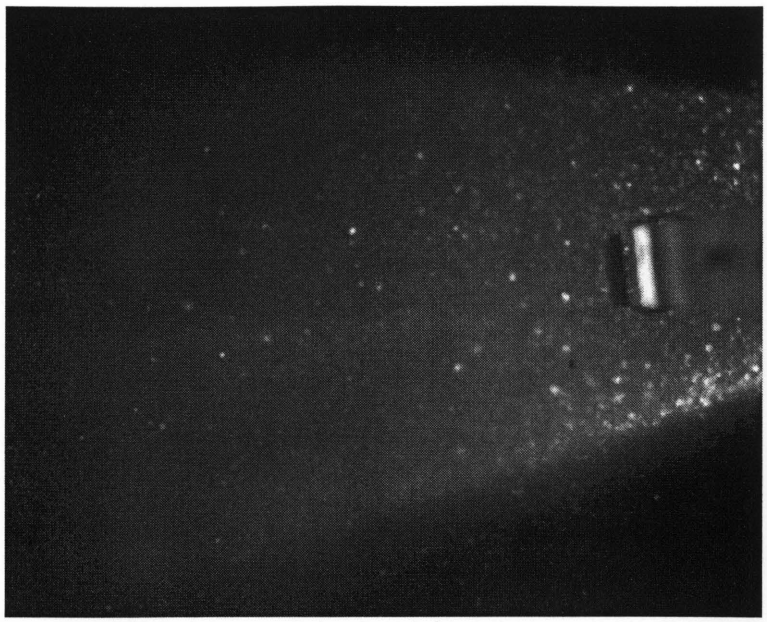

a) the first image before a relative movement in the pile

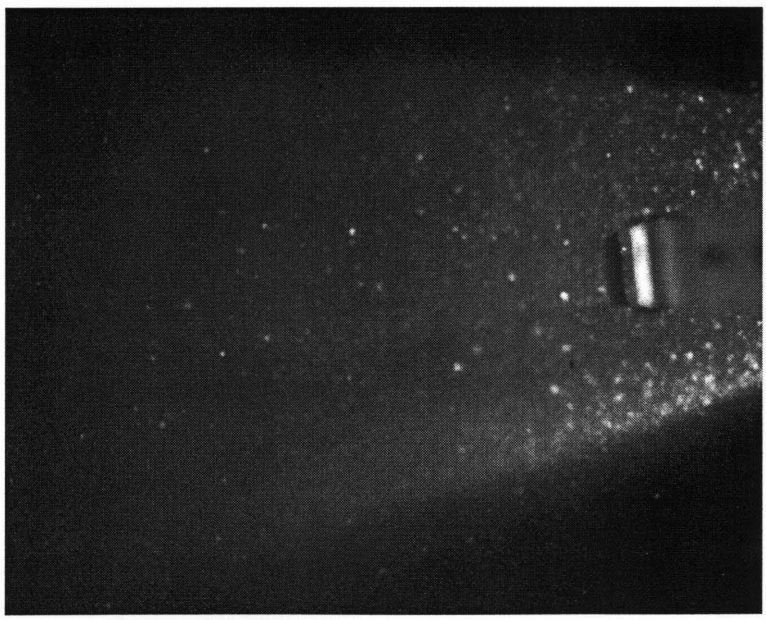

b) the second image after a relative movement in the pile

Figure 6.17 Two consecutive images for the hollow square pile (at stage C)

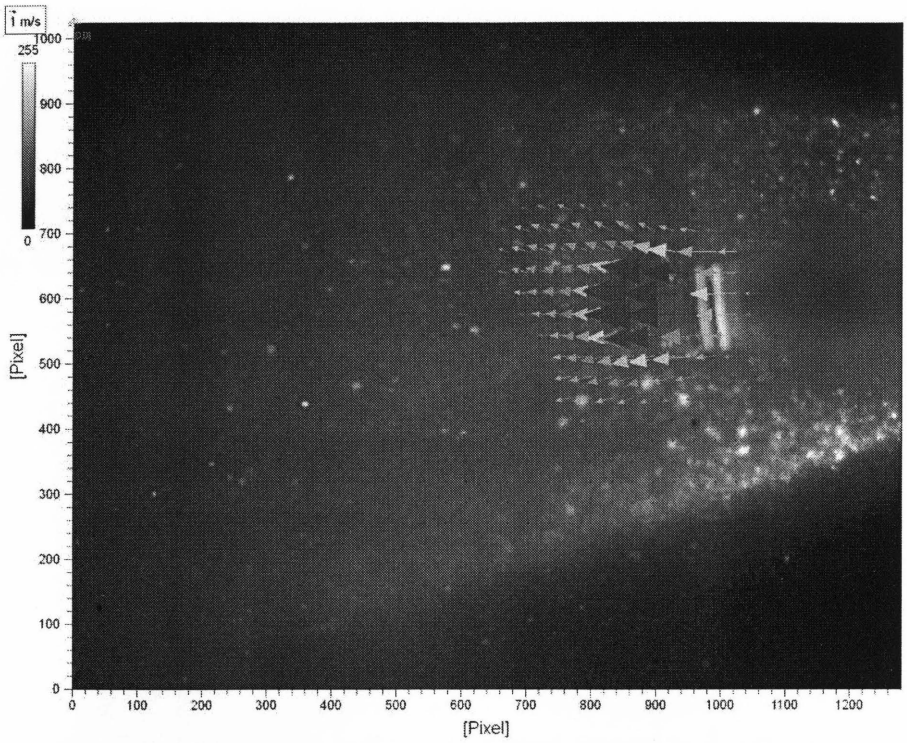

Figure 6.18 Soil deformation pattern (pile image inserted as the background)

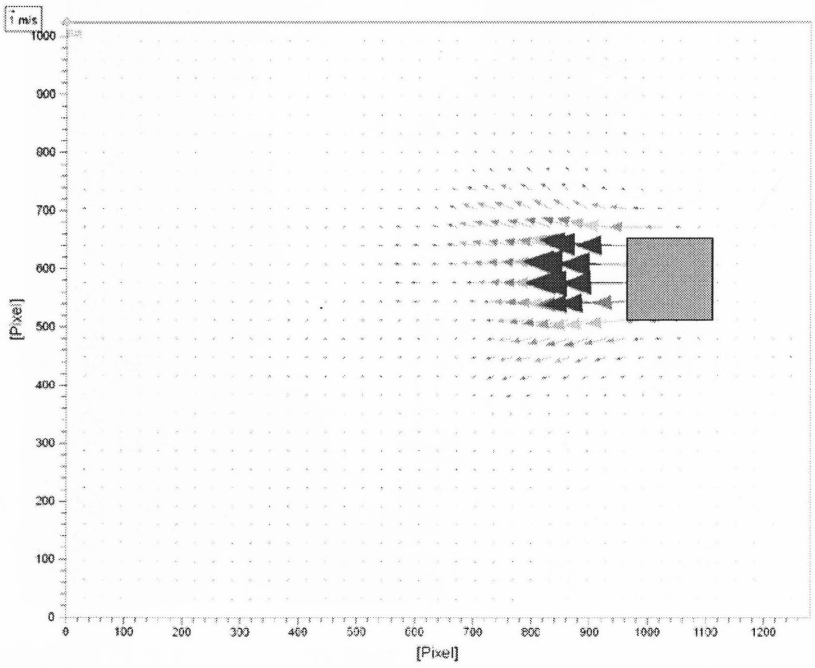

Figure 6.19 Deformation pattern (without the actual background)

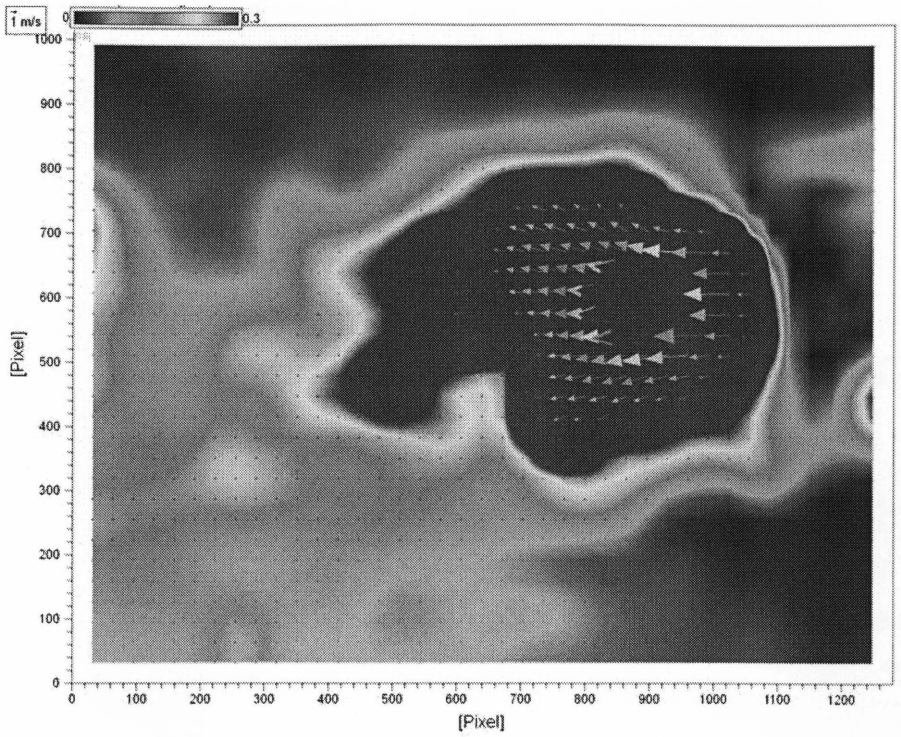

Figure 6.20 Shaded displacement contour

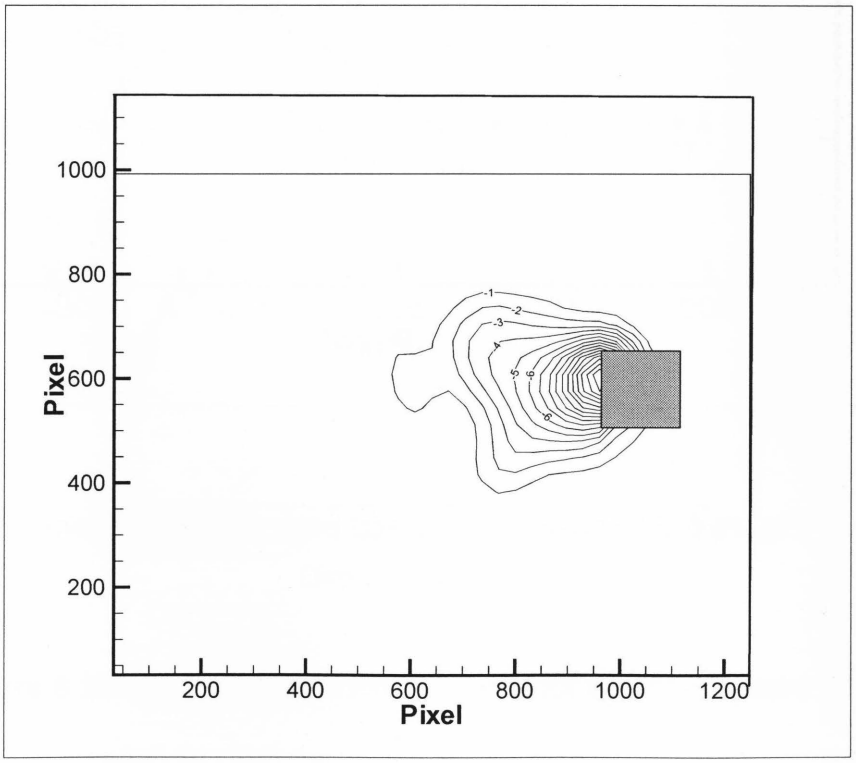

Figure 6.21 Displacement contours

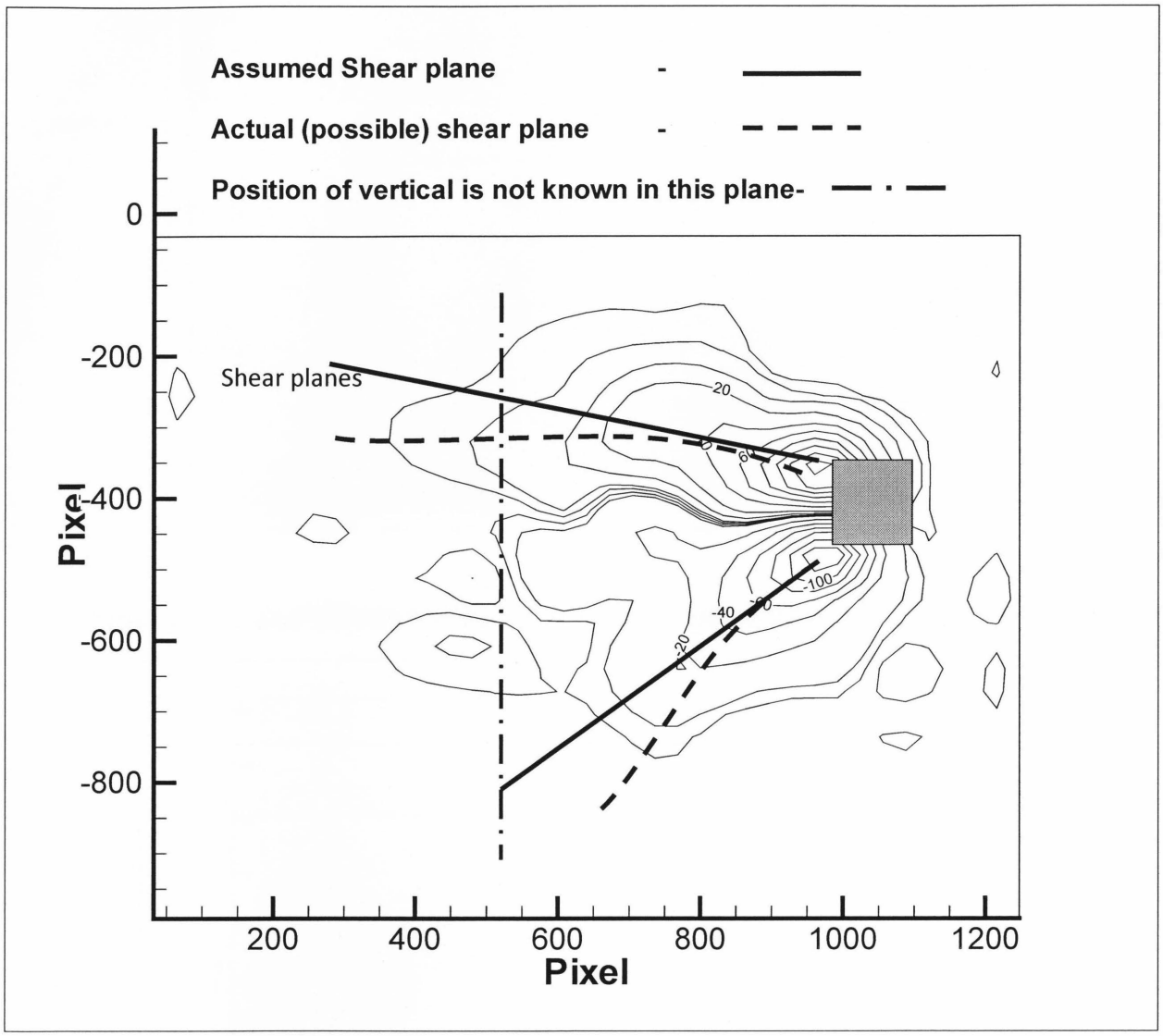

Figure 6.22 Shear contours and potential failure plane

6.5 SOIL MOVEMENT ALONG THE VERTICAL PILE

The test was repeated for all three types of piles to observe the soil movements in the vertical plane along the pile and the camera position was changed accordingly. The images were taken and analyzed with the PIV software. The results were not very useful in the determination of the complete shear envelope. It could be due to the image errors caused by the light reflection, camera position and the laser intensity. Therefore it is not possible to make a comment on the complete shear envelope as explained in chapter 2.

The hollow cubical shaped pile displayed better results compared to the other shaped piles, but still this result hardly makes any contribution to determine the possible shear plane in the elevation. Therefore the results for the hollow shape are presented only for demonstration purpose.

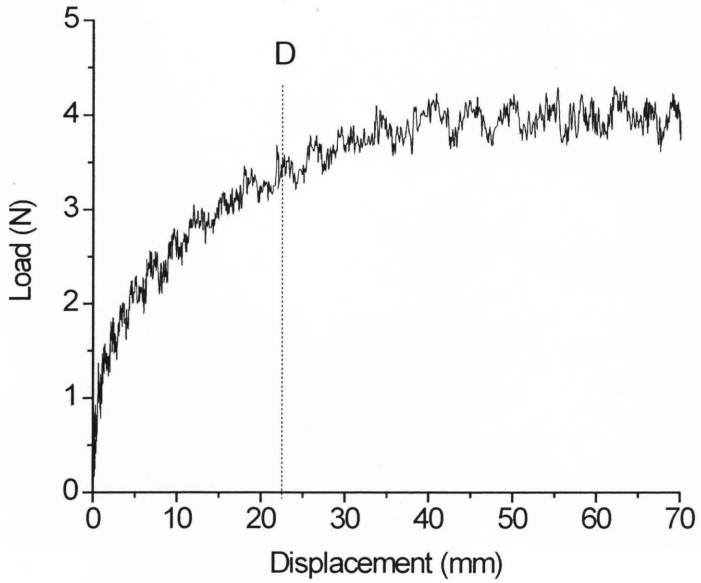

Figure 6.23 Load vs. displacement curve for a hollow square pile

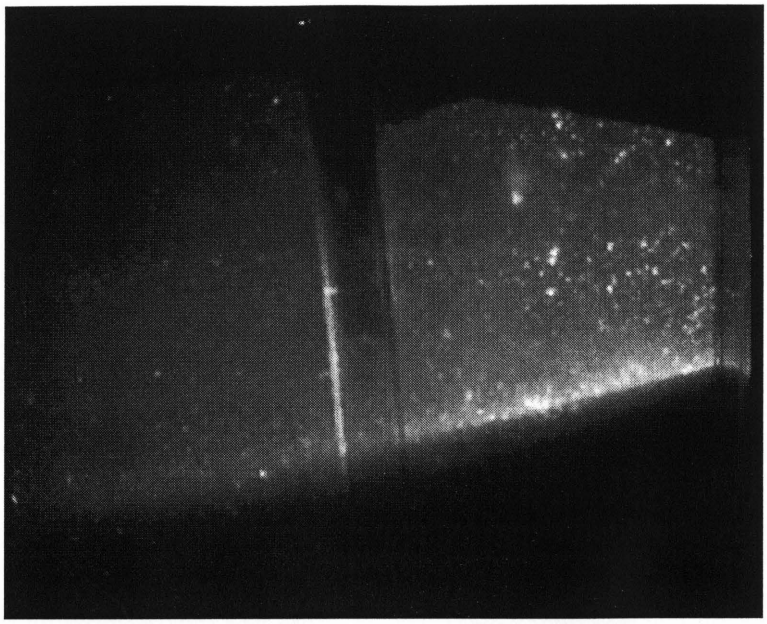

a) the first image before a relative movement in the pile

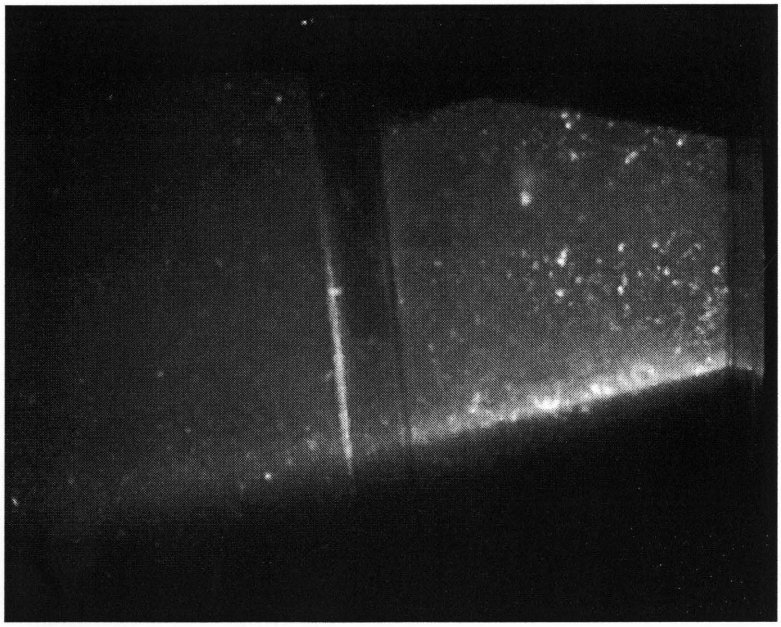

b) the second image after a relative movement in the pile

Figure 6.24 Adjacent Images for hollow square piles (at stage D)

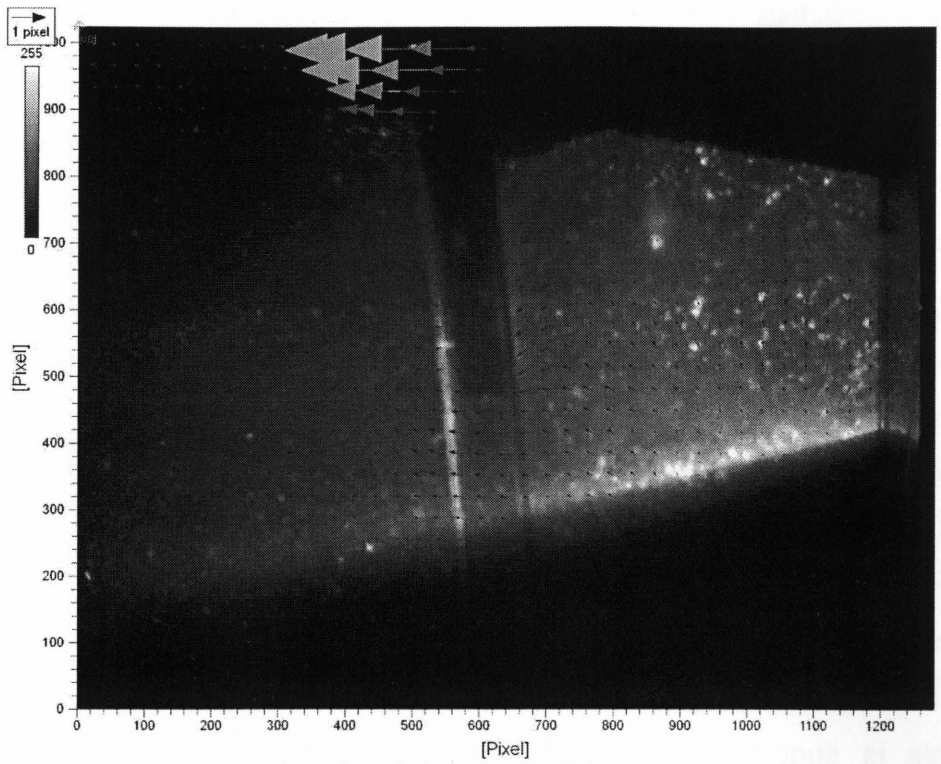

Figure 6.25 Soil deformation pattern (pile image inserted as the background)

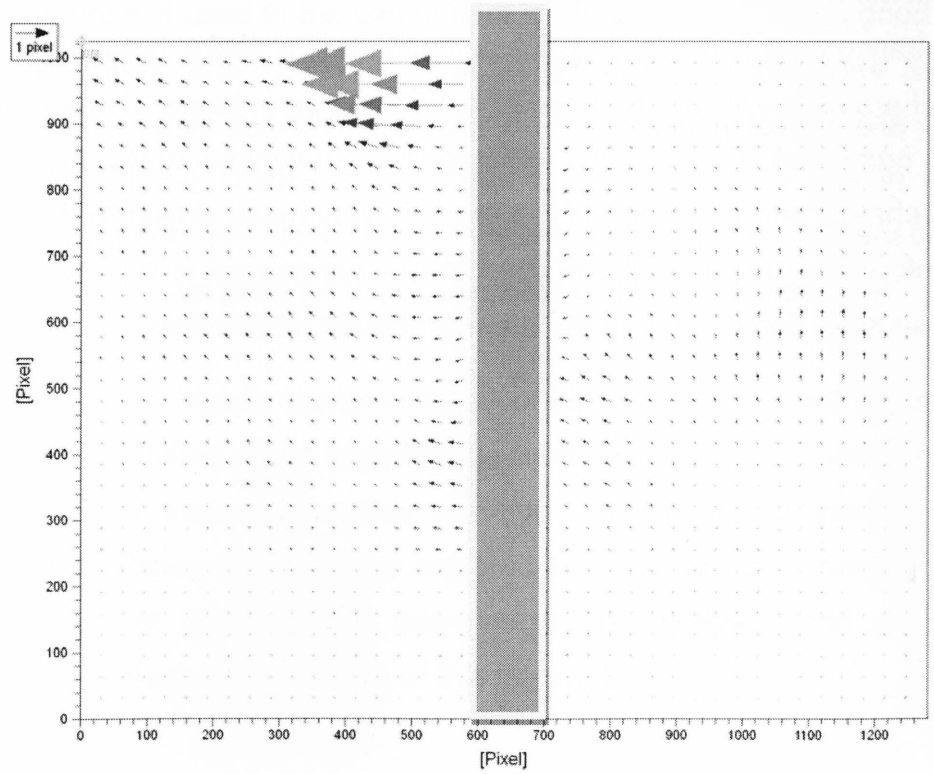

Figure 6.26 Deformation Pattern (without the actual background)

6.6 CONCLUSIONS

The results for the horizontal plane has a good agreement with the published information and assumptions used to explain the actual behavior of soil around a laterally loaded vertical pile (Figure 2.4)

The vertical plane results are not very good to get a full picture of the shear planes and deformation patterns. This could be mainly due to the errors in the images caused from light reflection. The camera distance was much higher than that of the horizontal case in order to capture a wider area in the vertical case. The Maximum penetration of the laser used is 15 cm and therefore the laser intensity in the frontal area of the pile is much less compared to that of close to the walls. The diverging shape of the laser sheet has a greater effect on the images in the vertical case.

In the future, it is expected to improve this experimental set-up for observing and imaging the complete three-dimensional behavior of the sample to get more reliable results. This is suggested by slicing the sample both vertically and horizontally simultaneously and imaging with two synchronized cameras. That may give a better picture about the development of shear planes.

The transparent soil has a good potential in the future researches. It exhibits geotechnical properties similar to those of natural sands in terms of shear strength and deformation properties. The load and displacement relationship during the tests reflect a non-linear behavior and the shape of the graph is very much similar to that of loose fine sand. Therefore, the transparent soil used in this experiment is a good representative for the real sand for demonstrating the unseen internal movements.

CHAPTER 7

CONCLUSIONS AND RECOMMENDATIONS

7.1 CONCLUSIONS

In the research, an internal sand displacement field around a laterally loaded vertical pile is visualized using transparent soil and digital image correlation (DIC). The shear strain and the displacement fields at a horizontal plane have a good agreement with the published data, but the results from a vertical plane are not as good as the ones from the horizontal plane due to experimental errors.

7.1.1 Transparent Synthetic Soils

Transparent soil used in the experiment to simulate sand has a good potential in the future researches, due to the fact that Its geotechnical properties are similar to natural sand. The load vs displacement curves of the laterally loaded pile show a non-linear behavior and the shape of the graph is very similar to that in loose sand. Therefore, transparent soil used in this experiment may be a reasonably good representative for the real sand for the observation of internal movements.

But due to the higher compressibility of silica gel compared to natural sand, special caution is required when applying the model results to the actual geotechnical problems. Therefore more researches may be required for preventing a potential misinterpretation. Researches can be explored in many aspects, including the critical stress parameters of this material, non-dimensional analysis, and surface charge influence on the geotechnical behavior of this material.

7.1.2 DIC Technique

DIC is shown to be a reliable technique for measuring deformation in transparent synthetic soil mass. The accuracy of the technique is dependent on the displacement magnitude and the window size used in the analysis. In general, the technique provides more accurate results for small displacements and large window sizes

7.2 TECHNICAL LIMITATIONS

Transparent synthetic soil model used in this research was limited in size due to loss of transparency with the increased thickness. This is caused by the presence of the impurities in the solid particles and mismatch in the refractive index of silica gel and pore fluid. The laser penetration depth was limited to 15 cm due to the strength of laser used and the results from the vertical plane have been heavily affected by this factor. With this experimental set-up only the in-plane displacement can be measured. The presence of out-of-plane movement also affects the accuracy of DIC for in-plane measurements. The other critical factor is breakage of silica gels, which may limit the types of problems that can be simulated using transparent silica gel.

7.3 IMPROVING THE IMAGING SYSTEM PERFORMANCE

The imaging system performance can be improved for better results and wider applications by using high power lasers. Currently the research is limited to the available laser source (35 mW). The laser wave length is a governing factor in laser light diffusion and penetration into the specimen. A green laser might provide deeper penetration than the red laser.

The silica gel used in this experiment is manufactured as an absorbing agent and it has some impurities. Therefore it is important to find a silica gel produced for specific experimental work. More investigation of the geotechnical properties of transparent synthetic soil is required for better system performance. Further investigation may include; more properties of the available transparent synthetic soil such as soil fabric and particle microstructure. Further studies are needed to evaluate the stress level that causes the breakage and its impact on the model failure mechanism. New materials; for

example fused silica, may have better properties than silica gel, thus it may improve the modeling system performance.

7.4 RECOMMENDATION FOR FUTURE WORK

The research presented in this thesis can be considered as an important step towards developing a new experimental technique that may have far reaching impact in modeling geotechnical engineering problems. There is a lot more work that needs to be done such as, improving the performance of imaging system, further investigation of the geotechnical properties of transparent soils.

There are high hopes of applying this technique for three-dimensional (3D) measurements. The application of transparent soil system in 3-D measurements, require to design for a mobile setup that can illuminate various cross sections in the soil model, using laser light sheets. The system should ideally be associated with a computer controlled image acquiring system and two synchronized cameras.

REFERENCES

Adrian, R.J., "Particle-Imaging Techniques for Experimental Fluid Mechanics", *Annual Review of Fluid Mechanics*, 1991, vol. 23, pp. 261-304.

Allersma, H., "Using Imaging Technologies in Experimental Geotechnics", *Proceeding 2, International Conference on Imaging Technologies, Techniques and Applications in Civil Engineering*, ASCE, 1997, pp. 1–9.

Ashour, M., Norris, G., Piling, P.," Strain Wedge Model Capability of Analyzing Behavior of Laterally Loaded Isolated Piles, Drilled Shafts and Pile Groups", *Journal of Bridge Engineering*, July/ August 2002.

Barron, J., Fleet, D. and Beauchemin, S.,"Performance of Optical Flow Techniques", *International Journal of Computer Vision*, 1994, vol.12, pp.43-77.

Bowman, E.R.," Investigation of The Lateral Resistance to Movement of a Plate in Cohesionless Soil", *Thesis, University of Texas*, Austin, Texas, 1958.

Cox, W.R., Reese, L.C. and Grubbs, B.R.," Field Testing of Laterally loaded piles in Sand",*Sixth Annual Offshore Technology Conference* , Houston, Texas, 1974.

Das, B. M., *Fundamentals of Geotechnical Engineering*, third edition, 2008, Thompson Learning, pp. 243-276.

Das, B M, *Principles of Foundation Engineering*, sixth edition, 2007, Thompson Learning, pp. 491-584.

Dunnavant, T.W. and O'Neil, M.W.,"Experimental p-y Model for Submerged Stiff Clay", *Journal of Geotechnical Engineering*, November,1989, vol.115, pp. 1681.

Fleming, K., Weltman, A., Randolph, M., Elson, K., Piling Engineering, third edition, 2009, Taylor & Francis, pp. 144-165.

Giachetti, A.,"Matching Techniques to Compute Image Motion." *IEEE Image Vision Computing*, 2000, vol.18, pp.247-260.

Glesser, M., "Lateral Load Test on Vertical Fixed-Head and Free-Head Piles", *Symposium on Lateral Pile Load Tests*, 1953.

Heteny, M., Beams on Elastic Foundation, The University of Michigan Press, Ann Arbour, 1946, section 56.

Huang, T.S. and Tsai, R.Y., Image Sequence Analysis and Motion Estimation, T.S. edition, 1981,Springer-Verlag, pp. 1-18.

Iler, R., The Colloid Chemistry of Silica and Silicates, Cornell University Press, Ithaca, New York, 1955.

Iskander, M., Liu, J. and Sadek, S., "Transparent Amorphous Silica to Model Clay", *Journal of Geotechnical and Geo-environmental Engineering*, March 2002.

Iskander, M., Sadek, S. and Liu, J., "Soil Structure Interaction in Transparent Synthetic Soils Using Digital Image Correlation", *Proceedings of TRB*, 2003.

Iskander, M., Lai, J., Oswald, C. and Mannheimer, R. "Development of a Transparent Material to Model the Geotechnical Properties of Soils." *GeotechnicalTesting Journal*, ASTM ,1994, pp. 425–433.

Iskander, M., Sadek, S. and Liu, J.,"Optical Measurement of Deformation Using Transparent Silica Gel to Model Sand", *International Journal in Physical Modelling in Geotech*, 2002b, pp. 27- 40.

Kihm, K.D., "Laser speckle photography technique applied for heat and mass transfer problems." Advances in Heat Transfer, 1997,vol. 30, pp. 255-311.

Konagai, K. C., Tamura, P., Rangelow and Matsushima, T.," Laser-Aided Tomography : A Tool for Visualization of Changes in the Fabric of Granular Assemblage," *Proceedings JSCE, Structural Engineering, Earthquake Engineering*, 1992, vol. 9, pp.193-201.

Kuhlemeyer, R. L.,"Static and Dynamic Laterally Loaded Floating Piles", *Journal of the Geotechnical Engineering Division*, February 1979, vol. 105, pp. 289-304.

Lamb, T. and Whitman, R., Soil Mechanics, 1969 , John Wiley, New York.

Liu, J. and Iskander, M., "Adaptive Cross correlation for imaging Displacements in Soils." *Journal of Computing in Civil Engineering*, ASCE ,2003.

Liu, J., Iskander, M. and Sadek, S., "Optical Measurement of Deformation Under Foundations Using a Transparent Soil Model." *Proceedings of International Conference on Physical Modeling in Geotechnics*, 2002, pp. 155-159.

Liu, J., Iskander, M and Sadek, S., "Consolidation and Permeability of Transparent Amorphous Sillica ", *Geotechnical testing journal*, 2002, vol.26.

Mannheimer, R. and Oswald, C., "Development of Transparent Porous Media with Permeabilities and Porosities Comparable to Soils, Aquifers, and Petroleum Reservoirs" Ground Water, 1993, pp.781-788.

Markandey, V., Reid, A. and Wang, S., "Motion Estimation for Moving Target Detection." *IEEE Transactions on Aerospace and Electronic Systems*, 1996, pp.866 –874.

Matlock, H. and Reese,L.C., " Generalized Solutions for Laterally Loaded piles", *Journal of the Soil Mechanics and Foundations Division*, ASCE, October, 1960.

Matlock, H. and Reese, L.C., " Foundation Analysis of Offshore Pile- Supported Structures", *Proceedings of Fifth International Conference, International Society of Soil Mechanics and Foundation Engineering*, Paris, 1961. Vol 2.

Matlock, H.,"Correlations for Design Laterally Loaded Piles in Soft Clay", *Proceedings of Offshore Technology conference*, Houston, Texas, 1970, pp.577-594.

McClelland, B. and Focht, J.A.,"Soil Modulus for Laterally Loaded Piles, American Society of Civil Engineers, 1958, Vol. 123, pp. 1049.

Murchison, J.M and O'Neill, M.W., "Evaluation of P-Y Relationships in Cohesion-less Soils", *Proceedings of a Symposium Sponsored by the ASCE Geotechnical Division and a Session Sponsored by the ASCE Technical Council on Codes and Standards in Conjunction with the ASCE National Convention*, San Francisco,California,October,1984,pp.174-191.

Parker, F., Reese,L.C., "Lateral Pile-Soil Interaction Curves for Sand", *Sixth Annual Offshore Technology Conference*, Houston, 1974.

Poulos, H. G.," Behavior of Laterally Loaded Piles:Single Piles",*Journal of the Soil Mechanics and Foundations Division*, May 1971, Vol. 97,pp. 711-731.

Randolph, M. F.,"Response of Flexible Piles to Lateral Loading", *Geotechnique*, June 1981, . Vol. 31, pp. 247-59.

Reese, L.C., Cox, W.R. , Koop, F.D. and Lawrence and – Allision Associates, "Analysis of Laterally Loaded Piles in Sand", *Sixth Annual Offshore Technology Conference*, Houston, Texas, May 6, 1974.

Reese, L.C., Isenhower, W. M. and Wang, S., *Analysis and Design Shallow and Deep Foundations*, 2006, John Wiley & Sons Inc, pp.441-503.

Reese, L.C. and Matlock, H.," Non- Dimensional Solutions for Laterally Loaded Piles with Soil Modulus Assumed Proportional to Depth", *Proceedings of Eight Texas Conference on Soil Mechanics and Foundation Engineering*, Austin, Texas, 1956.

Reese, L.C. and Van Impe, W.F., *Single Piles and Pile Groups Under Lateral Loading*, First edition, 2000, Taylor and Francis, pp.320-368.

Reese, L.C., Welch, R.C.,"Lateral Loading of Deep Foundations in Stiff Clay" *Journal of Geotechnical Engineering Division*, ASCE, July 1975, pp. 633-649.

Reese, L.C., Cox, W.R. and Koop, F.,"Field Testing and Analysis of Laterally Loaded Piles in Stiff Clay," *Proceedings of Seventh Offshore Technology Conference*, Houston, 1975, Vol. 2, pp.671-690.

Sadek, S.G., "Soil Structure Interaction in Transparent Synthetic Soils Using Digital Image Correlation." Ph.D. Dissertation, 2002, Polytechnic University, New York, USA.

Sadek, S., Iskander, M. and Liu, J., "Accuracy of Digital Image Correlation for Measuring Deformations in Transparent Media." *ASCE Journal of Computing in Civil Engineering*, 2003.

Sadek, S., Iskander, M.G. and Liu, J.,"Geotechnical Properties of Transparent Silica", *Canadian Geotechnical Journal*, 39(1), pp.111-124.

Sowers, G.B.,Sowers G.F., *Introductory Soil Mechanics & Foundations*: Geotechnical Engineering Fourth Edition, New York, 1970, pp. 621.

Sphinx Adsorbent, Inc. *Granular Silica Gel Data Sheet*, 53 Progress Ave, 1993 Springfield, MA 01104.

Sutton,M., Chung, M., Peters, W., Chao, Y., McNeil,S. and Helm, J.," Determination of displacements using an improved digital correlation method",Iimage Vision Computing, 1983, Vol. 1, pp.133-139.

Terzaghi, K., "Evaluation of Coefficient of Subgrade Reaction", *Geotechnic*, 1955, vol.5.5., December, pp297-326.

Tomlinson, M. and Woodward, J., *Pile Design and Construction Practice*, fifth edition 2008, Taylor and Francis, pp. 420-468.

Weast, R., *Handbook of Chemistry & Physics*, 66th edition, 1986, CRC Press, Boca Raton,Florida.